AFRL-AFOSR-VA-TR-2016-0122

Sustainable Alloy Design Searching for Rare Earth Element Alternatives through Crystal Engineering

Krishna Rajan
IOWA STATE UNIVERSITY

02/26/2016
Final Report

Air Force Research Laboratory
AF Office Of Scientific Research (AFOSR)/ RTB1
Arlington, Virginia 22203
Air Force Materiel Command

REPORT DOCUMENTATION PAGE

Form Approved
OMB No. 0704-0188

PLEASE DO NOT RETURN YOUR FORM TO THE ABOVE ORGANIZATION.

1. REPORT DATE *(DD-MM-YYYY)*	2. REPORT TYPE	3. DATES COVERED *(From - To)*
13-02-2016	Final	11/15/12 - 11/14/15

4. TITLE AND SUBTITLE
SUSTAINABLE ALLOY DESIGN: SEARCHING FOR RARE EARTH ELEMENT ALTERNATIVES THROUGH CRYSTAL ENGINEERING

5a. CONTRACT NUMBER

5b. GRANT NUMBER
FA9550-12-1-0456

5c. PROGRAM ELEMENT NUMBER

6. AUTHOR(S)
Rajan, K.
Sinnott, S.
Saxena, S.
LeBeau, J.

5d. PROJECT NUMBER

5e. TASK NUMBER

5f. WORK UNIT NUMBER

7. PERFORMING ORGANIZATION NAME(S) AND ADDRESS(ES)
Iowa State University, 3609 Administrative Services Building, Ames, IA, 50011
University of Florida, 106 Rhines Hall, Gainesville, FL 32611
Florida International University, 11200 8th St., Miami, FL, 33199
North Carolina State University, Raleigh, NC 27695

8. PERFORMING ORGANIZATION REPORT NUMBER

9. SPONSORING/MONITORING AGENCY NAME(S) AND ADDRESS(ES)
Air Force Office of Scientific Research (AFOSR)
801 N Randolph St., Rm. 732
Arlington VA 22203

10. SPONSOR/MONITOR'S ACRONYM(S)

11. SPONSOR/MONITOR'S REPORT NUMBER(S)

12. DISTRIBUTION/AVAILABILITY STATEMENT
Distribution A- Approved for Public Release

13. SUPPLEMENTARY NOTES

14. ABSTRACT

The objective of this project was to identify new chemical substitutions for rare earth elements in high temperature alloys via an informatics based alloy design strategy that captures the "rational materials design" strategy by integrating atomistic and multi-scale modeling with unique synthesis and characterization experiments under extreme pressure / temperature conditions. We have successfully achieved the primary goal of this project by identifying 29 new rare earth free Co-based and Ni-based superalloys. This provides for the first time a pathway for searching and identifying elemental substitutions in alloy design that now offers a means for significantly enhancing the acceleration of new critical element substitutions. This BRI sponsored project has also established a new data driven methodology tracking the collective influence of the multiple attributes of alloying elements on both thermodynamic and mechanical properties of metal alloys. The search for elemental substitutions and/or additions needed to refine metal alloy compositions and enhance their properties is a classical problem in metallurgical alloy design. A major transformative result from this project is that we have for the first time established a unified mathematical formalism for identifying the pathways of chemical design of alloys that can simultaneously capture the complexity of interactions with thermodynamics, crystal structure and microstructure.

15. SUBJECT TERMS
Rare earth element replacement, Informatics, Rational design, Quantitative correlative spectroscopy and imaging, DFT, In situ high pressure mechanical property measurements, Superalloy design

16. SECURITY CLASSIFICATION OF:			17. LIMITATION OF ABSTRACT	18. NUMBER OF PAGES	19a. NAME OF RESPONSIBLE PERSON
a. REPORT	b. ABSTRACT	c. THIS PAGE			Krishna Rajan
U	U	U	SAR	49	19b. TELEPHONE NUMBER *(Include area code)* 716-645-1380

Reset

INSTRUCTIONS FOR COMPLETING SF 298

1. REPORT DATE. Full publication date, including day, month, if available. Must cite at least the year and be Year 2000 compliant, e.g. 30-06-1998; xx-06-1998; xx-xx-1998.

2. REPORT TYPE. State the type of report, such as final, technical, interim, memorandum, master's thesis, progress, quarterly, research, special, group study, etc.

3. DATES COVERED. Indicate the time during which the work was performed and the report was written, e.g., Jun 1997 - Jun 1998; 1-10 Jun 1996; May - Nov 1998; Nov 1998.

4. TITLE. Enter title and subtitle with volume number and part number, if applicable. On classified documents, enter the title classification in parentheses.

5a. CONTRACT NUMBER. Enter all contract numbers as they appear in the report, e.g. F33615-86-C-5169.

5b. GRANT NUMBER. Enter all grant numbers as they appear in the report, e.g. AFOSR-82-1234.

5c. PROGRAM ELEMENT NUMBER. Enter all program element numbers as they appear in the report, e.g. 61101A.

5d. PROJECT NUMBER. Enter all project numbers as they appear in the report, e.g. 1F665702D1257; ILIR.

5e. TASK NUMBER. Enter all task numbers as they appear in the report, e.g. 05; RF0330201; T4112.

5f. WORK UNIT NUMBER. Enter all work unit numbers as they appear in the report, e.g. 001; AFAPL30480105.

6. AUTHOR(S). Enter name(s) of person(s) responsible for writing the report, performing the research, or credited with the content of the report. The form of entry is the last name, first name, middle initial, and additional qualifiers separated by commas, e.g. Smith, Richard, J, Jr.

7. PERFORMING ORGANIZATION NAME(S) AND ADDRESS(ES). Self-explanatory.

8. PERFORMING ORGANIZATION REPORT NUMBER. Enter all unique alphanumeric report numbers assigned by the performing organization, e.g. BRL-1234; AFWL-TR-85-4017-Vol-21-PT-2.

9. SPONSORING/MONITORING AGENCY NAME(S) AND ADDRESS(ES). Enter the name and address of the organization(s) financially responsible for and monitoring the work.

10. SPONSOR/MONITOR'S ACRONYM(S). Enter, if available, e.g. BRL, ARDEC, NADC.

11. SPONSOR/MONITOR'S REPORT NUMBER(S). Enter report number as assigned by the sponsoring/ monitoring agency, if available, e.g. BRL-TR-829; -215.

12. DISTRIBUTION/AVAILABILITY STATEMENT. Use agency-mandated availability statements to indicate the public availability or distribution limitations of the report. If additional limitations/ restrictions or special markings are indicated, follow agency authorization procedures, e.g. RD/FRD, PROPIN, ITAR, etc. Include copyright information.

13. SUPPLEMENTARY NOTES. Enter information not included elsewhere such as: prepared in cooperation with; translation of; report supersedes; old edition number, etc.

14. ABSTRACT. A brief (approximately 200 words) factual summary of the most significant information.

15. SUBJECT TERMS. Key words or phrases identifying major concepts in the report.

16. SECURITY CLASSIFICATION. Enter security classification in accordance with security classification regulations, e.g. U, C, S, etc. If this form contains classified information, stamp classification level on the top and bottom of this page.

17. LIMITATION OF ABSTRACT. This block must be completed to assign a distribution limitation to the abstract. Enter UU (Unclassified Unlimited) or SAR (Same as Report). An entry in this block is necessary if the abstract is to be limited.

SUSTAINABLE ALLOY DESIGN: SEARCHING FOR RARE EARTH ELEMENT ALTERNATIVES THROUGH CRYSTAL ENGINEERING

Grant / Contract Number: FA9550-12-1-0456

Principal Investigator Name:

Krishna Rajan, Iowa State University
Susan Sinnott, University of Florida
Surendra Saxena, Florida International University
James LeBeau, North Carolina State University

Program Manager: Dr. Ali Sayir

Period of Performance: 15 November 2012 – 14 November 2015

Abstract

The objective of this project was to identify new chemical substitutions for rare earth elements in high temperature alloys via an informatics based alloy design strategy that captures the "rational materials design" strategy by integrating atomistic and multi-scale modeling with unique synthesis and characterization experiments under extreme pressure / temperature conditions. We have successfully achieved the primary goal of this project by identifying 29 new rare earth free Co-based and Ni-based superalloys. This provides for the first time a pathway for searching and identifying elemental substitutions in alloy design that now offers a means for significantly enhancing the acceleration of new critical element substitutions. This BRI sponsored project has also established a new data driven methodology tracking the collective influence of the multiple attributes of alloying elements on both thermodynamic and mechanical properties of metal alloys. The search for elemental substitutions and/or additions needed to refine metal alloy compositions and enhance their properties is a classical problem in metallurgical alloy design. Finding appropriate alloy chemistries based on a systematic exploration using either computational and/or experimental approaches is often guided by prior heuristic knowledge that harnesses expected trends captured in the periodic table that can influence phase stability and properties. A major transformative result from this project is that we have for the first time established a unified mathematical formalism for identifying the pathways of chemical design of alloys that can simultaneously capture the complexity of interactions of metrics associated with thermodynamics, crystal structure and microstructure. The implication of our work goes beyond the immediate goals of this project by providing a computational framework that is generic enough to integrate data from many different length scales and as such can accommodate the addition of data associated with microstructure, processing and environmental response of alloys. This approach can be applied to many material systems and design objectives important to the Air Force. This is project has also demonstrated how informatics methods can help integrate data from computational materials science modeling, imaging and materials characterization techniques This project has also made significant contributions in advancing methodology and technique based research including: high throughput first principles calculations, ultra-high resolution quantitative correlative microscopy (integrating STEM and APT) and in –situ property characterization (high pressure/ high temperature X-ray studies)

I. Introduction, collaboration and accomplishments:

Major activities:

- Unique integration of informatics, mechanical properties at extreme conditions, computational modeling, and atomistic scale chemical imaging.

Major accomplishments:

1. **New informatics approaches for solute design of new alloy chemistries**. This work identified pathways to new chemical substitutions for rare earth elements in high temperature Co and Ni superalloys via an informatics based design strategy that involves coupling graph theoretic mapping coupled with dimensionality reduction. We identified 29 new Co-base and Ni-base alloys (Listed in Table 1) through this approach, significantly expanding the possibilities of RE free high temperature alloys. This approach can be applied to other materials and design objectives, and therefore can accelerate the design process for numerous Air Force applications.

2. **Quantitative correlative spectroscopy and imaging.** Experimental analyses (in-situ x-ray diffraction (XRD), STEM and APT microscopy) techniques and characterization have been developed, using Ni-Co-Al-Ti system (identified through informatics approach) as a test bed.

3. **Integration of DFT calculations and informatics for high throughput modeling of 'virtual' alloys**. By combining DFT calculation outputs with informatics analyses, we are able to rapidly predict site substitution of new chemical additions. With this integrated analyses, we identify the crystal chemistry of new compounds, thereby identifying compounds that have same behavior as those containing critical elements without requiring experimental fabrication. We have expanded this approach to predict Co and Ti site preference for a quaternary alloy $Ni_3Al(Co,Ti)$.

4. **Developed new charge optimized many-body (COMB) potentials for Ni alloys.** COMB3 potential was developed for Ni-Al system. This potential shows good agreement with experimental and DFT results. The Ni_3Al-Al_2O_3 interface was then examined using COMB3 potential. This provides a new approach for exploring interfacial chemistries / properties as a function of chemical substitutions.

5. **In-situ high pressure XRD and nanoindentation enabled the measurement of mechanical properties due to chemical additions to Ni-base and Co-base alloys**. With Cr addition, a decrease in compressibility is observed. Whereas, in the case of B-doping, B segregates to the grain boundaries which hinders the movement of defects and dislocations between grains causing an increase in bulk modulus and a decrease in shear modulus. We have identified that the grain boundary strengtheners improve the strength and ductility more than the lattice site

substituent. Further, measurements of Ni-Co-Al-Ti was made and correlated with the other research thrusts.

6. **Developed new enhanced imaging analysis methods for both STEM and APT imaging.** Imaging of intermetallics have enabled the capability to probe strain accurately and precisely at the atomic scale via STEM imaging. In parallel we have developed the first quantitative uncertainty assessment methods that can be standardized. These capabilities are essential to investigate strain between phases and the influence of chemical pressure at the unit cell level. With this approach, direct lattice strain has been measured in STEM images by correcting for drift and scan distortion.

This project has two major thrusts: alloy design and integration of the computational and experimental aspects, as shown in Fig. 1. In the first year of the program, we had a fundamental breakthrough in developing an informatics based computational strategy for solute selection in multicomponent alloys. From this work we identified promising high temperature Co-based alloy free of rare earth elements (Co-Al-Cr and Co-Al-Cr-Zr). In the second year, we validated those initial findings with DFT calculations, correlative microscopy between scanning transmission microscopy (STEM) and atom probe tomography (APT), and dynamic measurements under static and quasi-static extremes of pressure. In the third year, we have identified a list of rare earth free Ni-base and Co-base superalloys. Further, the integration of DFT and informatics produced a new computational approach for predicting substitute site occupancy in these superalloys. Finally, all research thrusts were applied in an integrated manner for testing and validating the selection of new superalloy chemistries derived from this project.

From the informatics analysis, we identified key chemistries to study through density functional theory (DFT) calculations, extreme pressure measurements, STEM and atom probe. This report describes the progress in developing and applying the various methodologies associated with each research thrust, as well as the integration of research thrusts as applied to the informatics-designed material. These accomplishments meet the project objectives as outlined in the proposal for design of new rare earth free Co and Ni-based superalloys and the integration of research thrusts for informatics guided DFT calculations and atom probe / STEM correlative microscopy.

Table 1: The following is a table summarizes the alloys identified as most promising in this project, thereby reducing the entire chemical search space to 29 alloys.

RE-free Co-Base Alloys	***RE-free Ni-Base Alloys***
Co-Ni-Al-Ti	Ni-Al-Hf-Zr
Co-Ni-Al-Ta	Ni-Al-Hf-Ti
Co-Ni-Al-Nb	Ni-Al-Zr-Ti
Co-Ni-Al-Mo	Ni-Al-Zr-V
Co-Ni-Al-V	Ni-Al-Zr-Nb
Co-Al-W-Re	Ni-Al-Hf-V
Co-Al-W-Os	Ni-Al-Hf-Nb
Co-Al-Mo-Rh	Ni-Al-Ti-Nb
Co-Al-Re-Ta	Ni-Al-Nb-Ta
Co-Al-Mo-Ru	Ni-Al-Ti-V
Co-Al-Re-Os	Ni-Al-Nb-Mo
Co-Al-Re-Ir	Ni-Al-V-Cr
Co-Al-Mo-Nb	Ni-Al-V-Ta
Co-Ni-Al-Re	Ni-Al-V-Mo
Co-Al-Re-Os	

The integration of the various program thrusts was accomplished through meetings, both live and virtual, and included individual and subgroup meetings, as well as regular web meetings attended by all participants, with each group presenting results and ideas. This included meetings in person by the attending participants at "Mapping the Materials Genome" workshop, organized by K. Rajan (February 4-7, 2014 in Santa Fe, NM), MRS 2014 conference (November 30 – December 5, 2014 in Boston, MA) and Microscopy and Microanalysis (M&M) 2015 (August 2 – August 6, 2015 in Portland, OR). At these meetings, results from this project were presented, both in oral presentations and poster presentations. Discussion among the teams at these meetings focused on the integration of results and the next steps in the research plan.

,

In the original proposal, we defined six primary design thrusts (Figure 1). The final Project Period of Performance was for three years, so those segments planned for Years 4 and 5 are not addressed in this project report. These included the expansion of our alloy design work into a usable database that can be used for future projects in the larger portfolio of AFOSR projects, addition of experiments and data that can account for materials processing parameters and other high temperature alloy systems such as Ti alloys, leverage our correlative microscopy studies into more automated tools to link characterization studies and finally explore the 'chemical pressure key new component that had been planned. The work we have done in the three year time period of this project however does establish the feasibility of these efforts in the future.

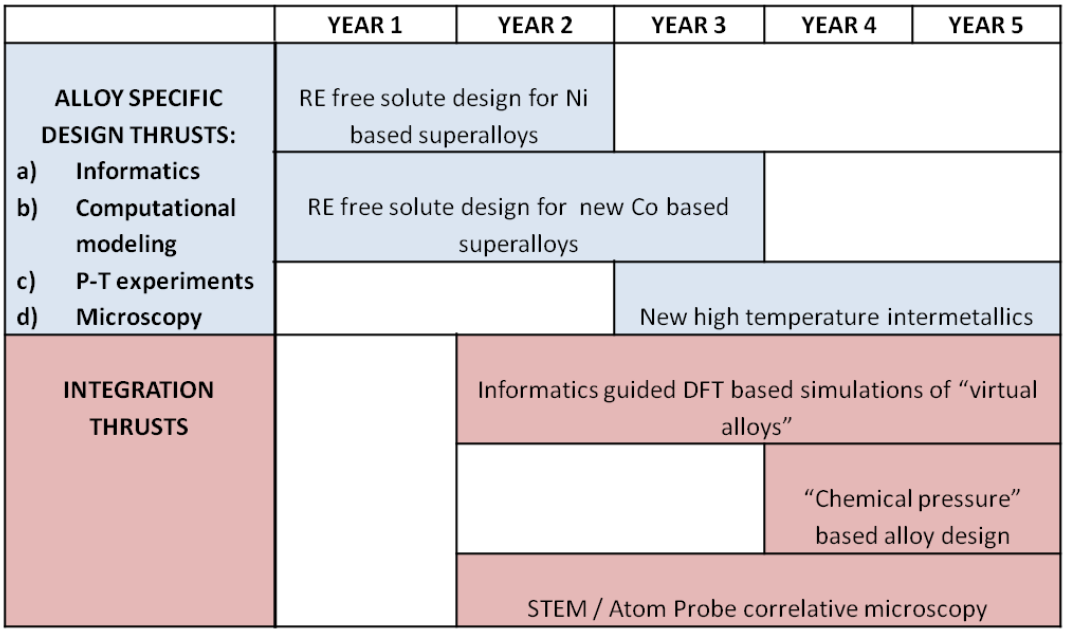

Fig. 1: The original project schedule from the proposal. This final report covers years 1 through 3.

This report is organized to correspond with the proposed project schedule: Section 2 – RE free solute design for Ni based superalloys; Section 3 – RE free solute design for new Co based superalloys; Section 4 – New high temperature intermetallics. Section 5 – Informatics guided DFT based simulations of "virtual alloys"; and Section 6 – STEM / Atom Probe correlative microscopy.

II. RE free solute design for Ni based superalloys

Optimal pathways, which are not captured in the periodic table, are extracted using the principle of the weighted graphs and criticality of elements. The weighted graph accounts for dissimilarity of elements, based on a rationale supported by existing theory. The challenge has always been to systematically

identify which elements would substitute for rare earths and provide for both oxidation resistance as well as mechanical properties. In order to develop this graph and analysis, we must develop a database, containing data from new computational tools and from STEM and high temperature microstructural measurements.

2.1. Informatics Identification of Rare Earth Substitutes

This work identifies pathways to new chemical substitutions for rare earth elements in high temperature Ni superalloys via an informatics based design strategy. Graph theoretic mapping coupled with dimensionality reduction is used to extract multiple non-linear pathways through a high dimensional data space, built by mapping discrete elemental data onto existing theories of alloy design to account for mechanical properties and thermodynamic stability in the course of elemental substitution. The challenge in design is the integration of various data types to develop a unified design rule. This integration is crucial for this project to include the data from both the computational and experimental aspects. A framework is presented for defining criticality of elements based on their physical and mechanical properties, thus providing a new definition for where the search for critical elements should occur (Figure 2).

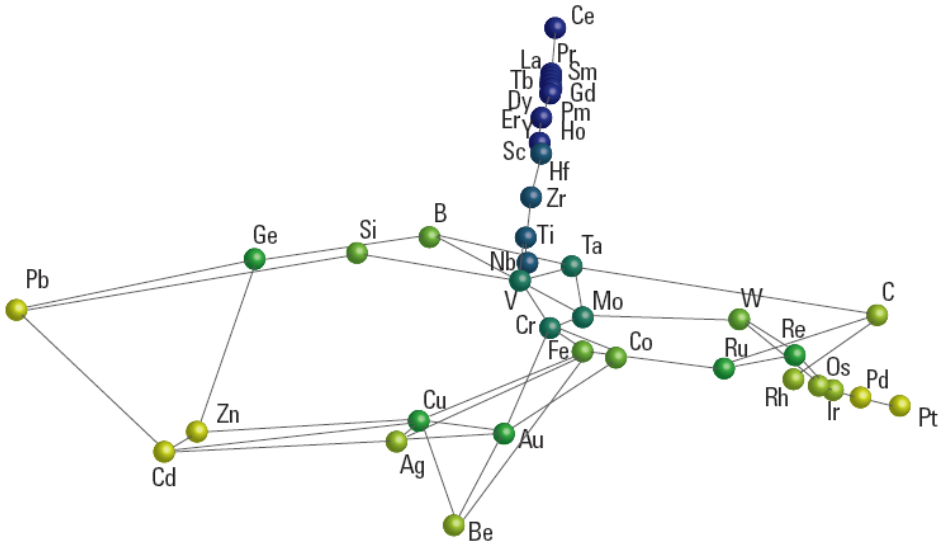

Figure 2: Graph network of effect of addititions to Ni alloys. Based on connections, density of nodes, and extracted design pathways, possible chemical substitutions are extracted, which are otherwise not obvious. For example, we find Ti, Zr, and Hf sit on the rare earth pathway, while Ta, Nb, and V sit at the intersection of this pathway and the plane containing non-rare earth elements. These elements thus provide a logical starting point for rare earth substitutions by defining elements that connect rare earths with the rest of the periodic table. The coloring of the spheres is based on the number of nearest neighbor connections separating that element from the RE elements.

The result (Figure 3) captures the unique behavior of REs, as identified by the clustering of the REs which reflects a similarity of behavior based on thermodynamics and structure. By identifying the number of connections between the RE cluster and additive element, we develop a metric for RE similarity as defined by the number of connections between the element and the cluster. This provides a single similarity metric which encompasses all of the properties. As shown in the figure, this provides a periodic table for RE replacement which does not track with atomic numbers. The final selection of descriptors was selected to achieve the highest connectivity within the RE elements. Further, this similarity mapping captures the changes in free energy formation related to oxidation, the change in solvus temperature, and the stability, with the higher similarity metric corresponding with most desired addition. Also, our similarity mapping captures the changes in free energy formation related to oxidation, the change in solvus temperature, and the stability, with the higher similarity metric corresponding with the most desired addition. This approach identifies Ti, V, Cr, Zr, Nb, Mo, Hf, and Ta as potential substitutes.

An additional consideration which must be made is that those elements have high availability as well. Therefore, we employ a second screening which is based on the possibility of substituting an element with another element with minimal effect. This is based on all uses of a material, whether in terms of processing and machinability or chemical characteristics or environmental properties [1]. Therefore, he defined the ability to substitute an element. We use this metric as our economic screening criteria with the logic that if availability of an element because a hurdle that other alternatives exist. That is, the more potential for maintaining the benefits over time of an additive increases its economic viability.

The integration of the graph theory derived similarity and economic screening provides a full exploration of the chemical search space. From this economic screening we identify Nb, Hf and Ta as the best rare earth substitutes in terms of maintaining engineering property. By combining the reported RE containing Ni alloy chemistries with these three substitutes, we identified new RE free Ni-base alloys (Table 2). The chemistry is defined by substituting the RE elements with Nb, Ta and/or Hf. Highlighted in this figure is the small quantities of RE added due to the formation of secondary phases at higher quantities. In these new alloys, the RE substitutes can likely be added at higher quantities, thereby further enhancing the alloying benefit.

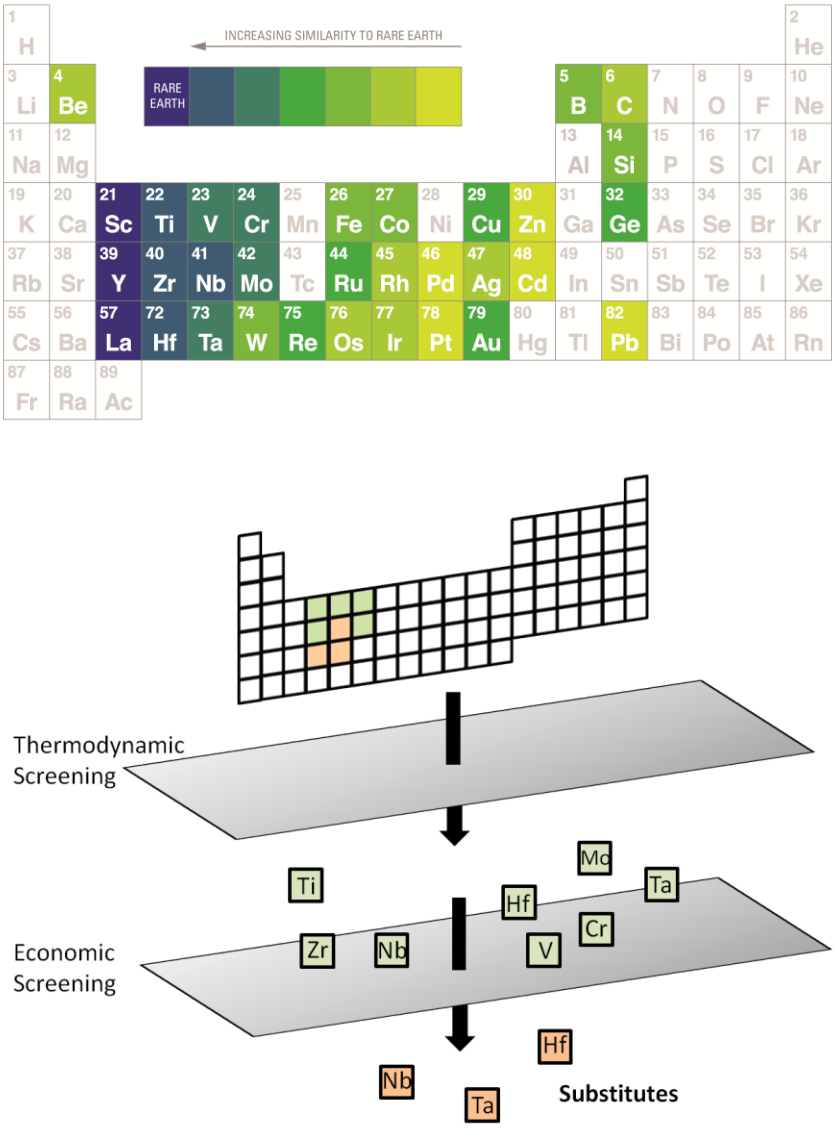

Figure 3. (Top) A similarity metric derived from a graph network for comparing the similarity of an addition to Ni alloy as that of a RE provides a similarity table which does not map with the periodic table. When further design characteristics, such as the separation of properties on oxidation by Gibb's free energy of alumina formation, are considered the multicomponent chemistries are identified. (Bottom) Summary of the results of the screening of Ni-based alloys. From the similarity metric we identified 8 elements which can best replace RE elements in terms of thermodynamic and mechanical properties. We have further screened these 8 elements based on availability and uniqueness of the elements, and have identified Nb, Ta and Hf (or combinations of these three elements) as the best substitutes for RE elements. This provides a major acceleration of superalloy design by addressing a longstanding roadblock of the trade-off between performance and economics.

Table 2. New RE free Ni-base alloys, based on replacing the RE in reported alloys with Nb, Ta and/or Hf. Beyond forming new alloys, the quantity of the RE free substitutes should be addable to quantities higher than the REs without forming secondary phases, thereby further enhancing the properties.

Alloy	X (Current)	X (New)
Ni-Al-X	Dy = 0.05% [9]	Ta, Hf, Nb
Ni-Al-X	Y = 0.06% [9]	Ta, Hf, Nb
Ni-Al-X	La = 0.09% [9]	Ta, Hf, Nb
Ni-Al-X	Ce = 0.01% [10]	Ta, Hf, Nb
Ni-Al-X	Ce = 0.025% [11]	Ta, Hf, Nb
Ni-Al-B-X	Ce = 0.02% [10]	Ta, Hf, Nb
Ni-Al-Cr-X	Ce = 0.05% [11]	Ta, Hf, Nb
Ni-Al-Cr-Nb-X	Y = 0.014% [12]	Ta, Hf
Ni-Al-Cr-Mo-Hf-X	Ho = 0.05% [13]	Ta, Nb

2.2. Development of Ni-Based Superalloy Database

2.2.1. Computational Modeling Thrust

Molecular Dynamics simulations using Charge Optimized Many-Body (COMB) potential

An interatomic potential for the Ni-Al system was developed [1] and is implemented in the open-source LAMMPS software distributed by Sandia National Laboratory. It allows users to perform Molecular Dynamics (MD) simulations on different phases of Ni-Al. This potential is also capable of simulating the Ni and Al elemental phases. Specifically, an Al potential was proposed elsewhere while the Ni potential is introduced here. The interatomic potential focuses on Ni_3Al and NiAl, with more emphasis on Ni_3Al, which is the γ' phase of the Ni-base superalloys and responsible for the high temperature performance of these alloys. Figure 4 shows the formation energy predicted by COMB3 and a comparison with EAM [Purja Pun G P and Mishin Y 2009 *Philos. Mag.* 89 3245-67] and DFT [Jain A *et al.,* 2011 *Phys. Rev. B* 84 045115]. The high mechanical strength is related to the unusual dislocation activity in the $L1_2$-structured Ni_3Al [1] due to the Stacking Fault energies and the Antiphase Boundary energies (APB) of the system. Therefore, one key feature of the interatomic potential is the ability to reproduce this behavior. Table 3 highlights these properties and a comparison with an EAM potential.

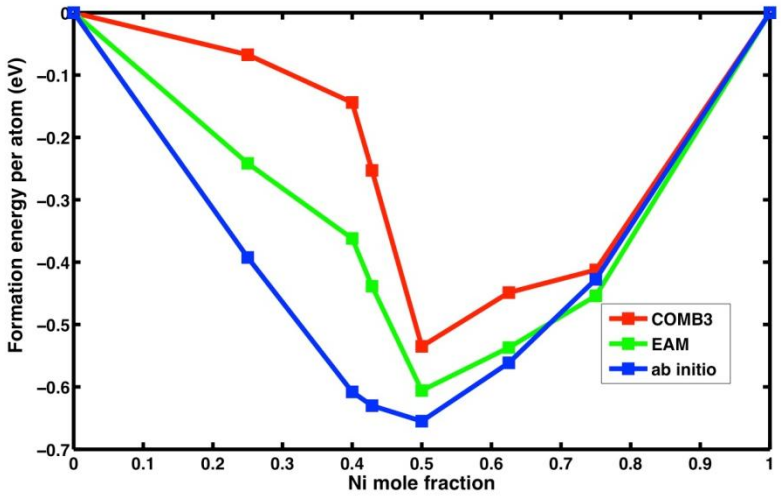

Fig. 4: Formation energy/atom for different Ni-Al phases as calculated from COMB3, EAM Pun-Mishin and DFT.

Table 3: Planar faults in Ni_3Al and their energies (mJ/m^2) from experiments, DFT, EAM and COMB3.

	Expt.[a]	*ab initio*[b,c]	EAM (Pun-Mishin)[d]	COMB3 (this work)
CSF (111)	235	225[b]	193	178
APB (111)	175	210[b]	249	311
APB (100)	104	121[c]	74	199

a- Karnthaler H P, Mühlbacher E T and Rentenberger C 1996 *Acta Mater.* 44 547-60,

b- Mryasov O N *et al,* 2002 *Acta Mater.* 50 4545-54,

c- Kohlhammer S, Fähnle M and Schoeck G 1998 *Scripta Mater.* 39 359-63,

d- Purja Pun G P and Mishin Y 2009 *Philos. Mag.* 89 3245-67

The current potential also is capable of including the oxygen interactions in the Ni-Al system and strengthens the suite of COMB3 potentials that are capable of simulating heterostructures. In this case, an intermetallic-ceramic interface was simulated. It has been shown in the literature that $Ni_3Al(111)$-$Al_2O(0001)$ interface is the most stable. The present potential is able to simulate the interface and provide equilibrium charge values on each species as it allows for dynamic charge equilibration. Figure 5 illustrates the interface as obtained from the MD simulations.

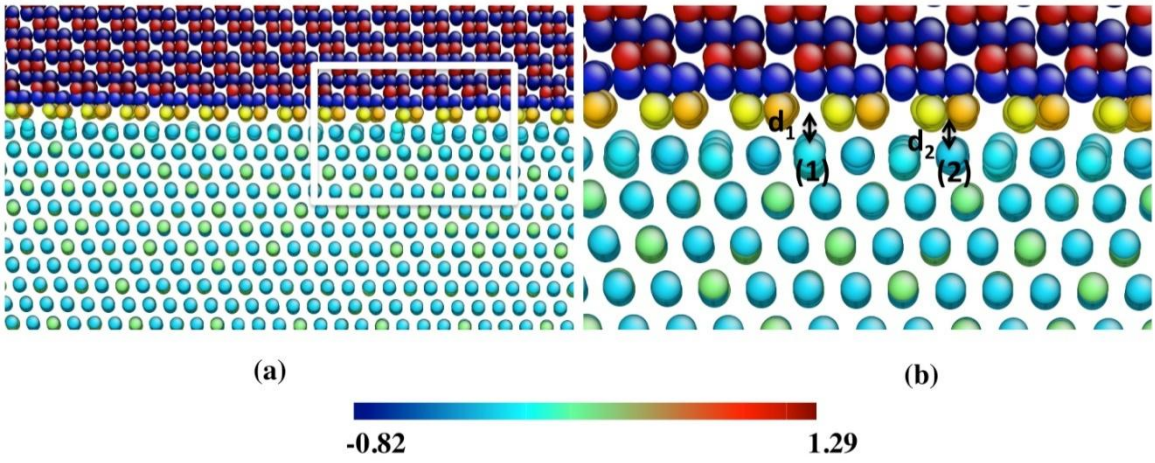

Fig. 5: (a) $Ni_3Al(111)$-$Al_2O_3(0001)$ interface with the atoms color-coded according to charge. (b) Close-up of the square from (a) to illustrate the variation of the interface distance at two different sites.

The predicted equilibrium distance between Ni_3Al and Al_2O_3 is 1.8 Å (d_1) at site (1) and 2.42 Å (d_2) at site (2) in Fig. 5 (b). It can be concluded that Ni atoms at site (1) from Ni_3Al are pulled towards the O atoms in Al_2O_3. Since at site (2) the Ni atoms in Ni_3Al have Al atoms from Al_2O_3 on the top, the distance is limited to 2.42 Å. The (d_1) distance computed from DFT was shown to be 1.86 Å for the Ni (111)-Al_2O_3 (0001) interface by Zhang *et al*. [2002 *Acta Mater.* 50 3803-16] and it was shown that the interface stability was attributed to the polarization of Ni atoms by O atoms on their top. The same argument could be applied to the Ni-rich intermetallic Ni_3Al (111) - Al_2O_3 (0001) interface. In this way, the present potential is able to provide different types of information about the behavior of Ni_3Al and other Ni-Al phases.

Damage at the Al_2O_3-Ni_3Al interface due to collisions with debris and particles is a common phenomenon in the moving parts of e.g., jet engines, composed of nickel superalloys. This damage is investigated with the present COMB3 potential for Ni-Al-O to determine the dominant atomic-scale mechanistic responses as a function of collision kinetic energy, interface structure, and system composition.

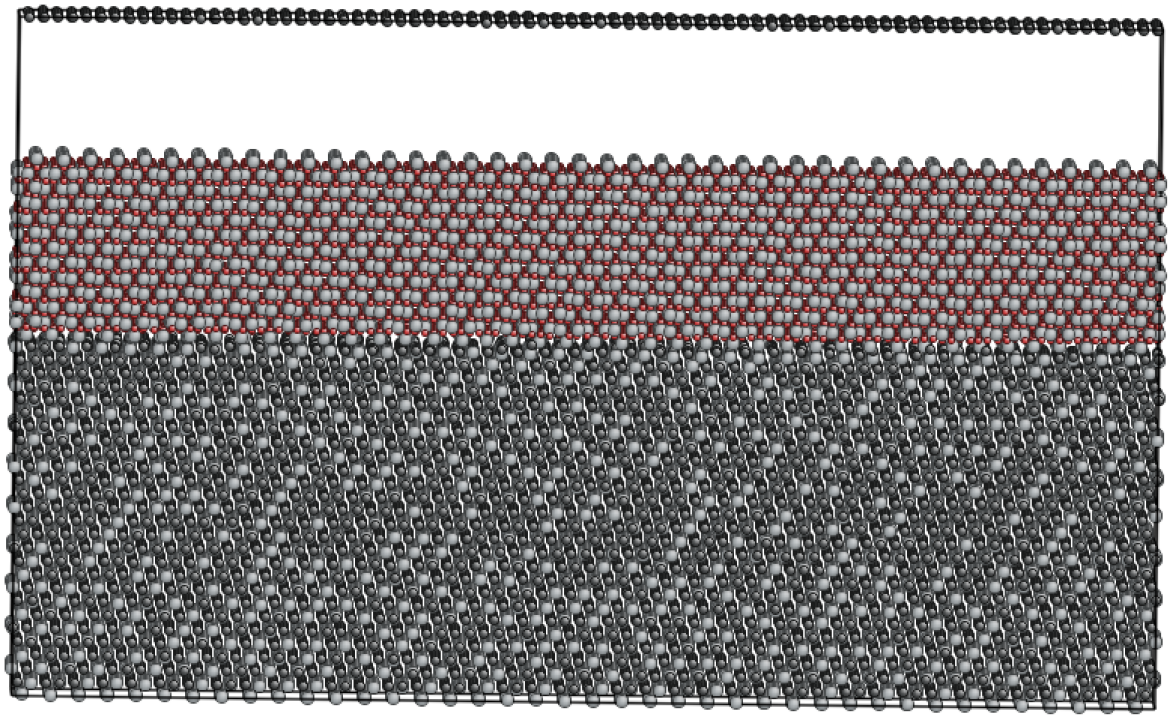

Fig. 6: Al_2O_3 (0001)-Ni_3Al (111) interface (light grey-Al, red-O, dark grey-Ni) of 139,320 atoms.

The simulations are carried out by providing an initial velocity to a small region of the surface (about 0.05 nm) such that the atoms have a net kinetic energy of around 400-600 eV. These conditions resemble those where a rigid particle strikes the interface and transfers its momentum. The simulation box has vacuum in the direction perpendicular to the interface. Figure 7 illustrates this scenario from a top-down perspective where the atoms are color-coded according to their kinetic energy and the area in the middle is the impact site.

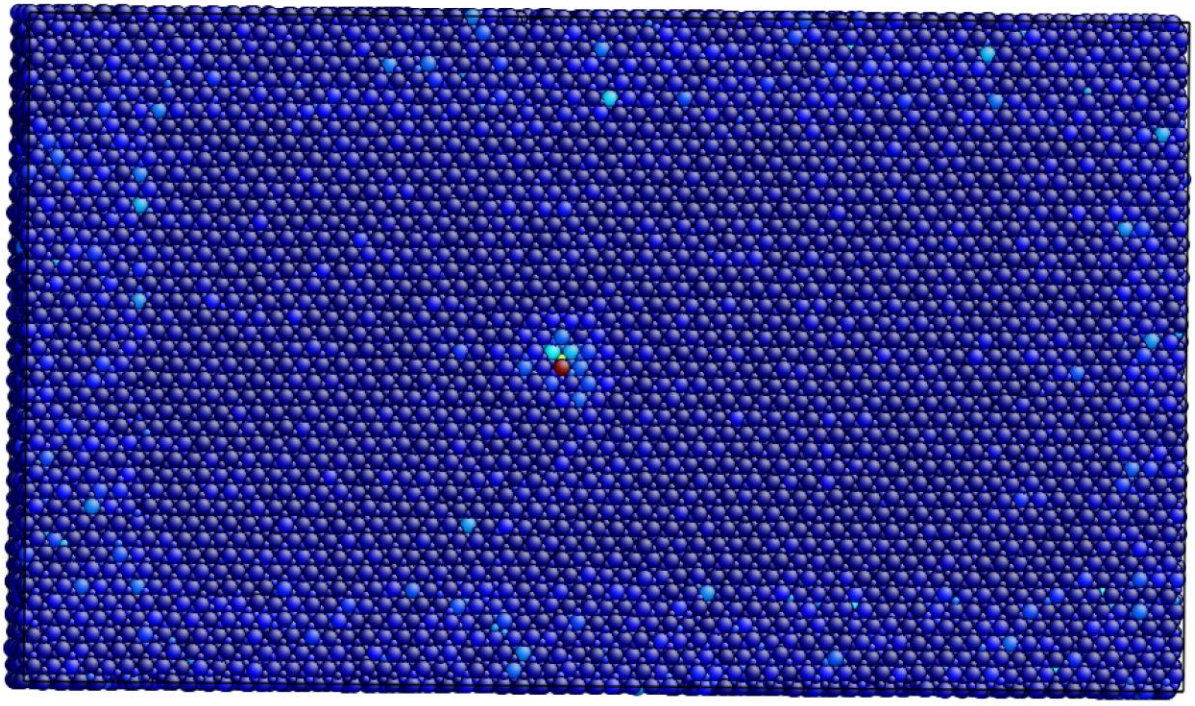

Fig. 7: Top-down view of Al_2O_3 (0001)-Ni_3Al (111) illustrating the impact site.

First-principles investigation of Ni_3Al(Co,Ti)

We previously considered the introduction of several dopants, B, Cr, Zr, Ce and La to Ni_3Al and their effects were investigated with respect to magnetic and elastic properties. It was also shown how the site preference of these dopants varies for a ternary alloy and was validated with the other results from the literature. Currently, quaternary alloy systems with Co and Ti are under investigation. Use of ATAT tool [http://www.brown.edu/Departments/Engineering/Labs/avdw/atat/] enables the examination of several combinations of alloy systems for a given concentration. For example, Co-Ti were placed in nearest neighbor sites in Ni_3Al, such as Al-Al, and their tendency to occupy these sites calculated, as illustrated in Figure 8. From the current calculations, Ni and Al sites are predicted to be preferred for Co and Ti occupation, respectively.

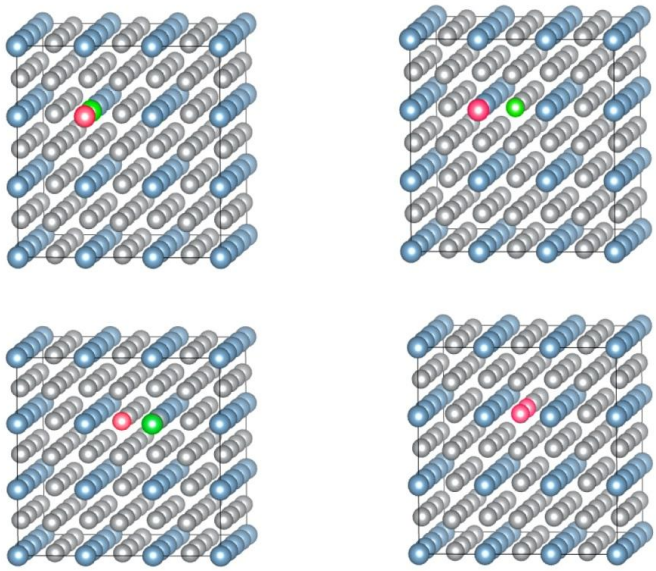

Fig. 8: A 3x3x4 supercell of Ni_3Al showing Co (red) and Ti (green) atoms at Al-Al, A-Ni, Ni-Ni and Ni-Al sites.

Current efforts are directed towards exploring the effects of concentration of these dopants using ATAT. In particular, Co is being investigated as the site preference of Co changes with its concentration in Ni_3Al. To study the occupation, we place Co in both (i) Al and (ii) Ni site and try to use cluster expansion using ATAT to look at the ground states. Basically, different configurations of Co atoms within Ni_3Al are considered to predict the most stable ground states for different Co concentrations. In other words, we are able to obtain a prediction of the convex hull with Ni_3Al at one end and Co_3Al/Ni_3Co at the other end. If we let Co substitute for Ni completely, the compound is Co_3Al whereas if Co occupies only Al sites, the compound is Ni_3Co.

The structures that are predicted to be ground states will then be used in Monte Carlo simulations at higher temperatures to account for the configurational entropy of the alloy and determine the resulting ground states as a function of temperature. It is expected that beyond a certain temperature limit all phases will exhibit a random distribution and form disordered systems regardless of composition.

2.2.2. P-T Experiments Thrust

Yield Strength of Ni-Al-Cr at high pressure

Ni based superalloy Ni-Al-Cr with γ and γ' phase was studied under high pressure up to 30 GPa using diamond anvil cell technique. In-situ x-ray diffraction data was collected on these alloys under hydrostatic and non-hydrostatic conditions. Cubic phase remains stable up to the highest pressure studied. Bulk modulus and its pressure derivative obtained from the volume compression of pressure data are K= 166.6±5.8 GPa with K' set to 4 under hydrostatic conditions and K= 211.3 ±4.7 GPa with K'

set to 4 for non-hydrostatic conditions. Using lattice strain theory, maximum shear stress 't' was determined from the difference between the axial and radial stress components in the sample. The magnitude of shear stress suggests that the lower limit of compressive strength increases with pressure and shows maximum yield strength of 1.8±0.3 GPa at 20 GPa. Further, we have also determined yield strength using pressure gradient method. In both methods, yield strength is found to increase linearly with applied pressure. The results are in good agreement with each other and with literature values at ambient conditions. Equation of state of Ni-Al-Cr system was obtained from the Pressure – volume data measured at various pressures under hydrostatic and non-hydrostatic data.

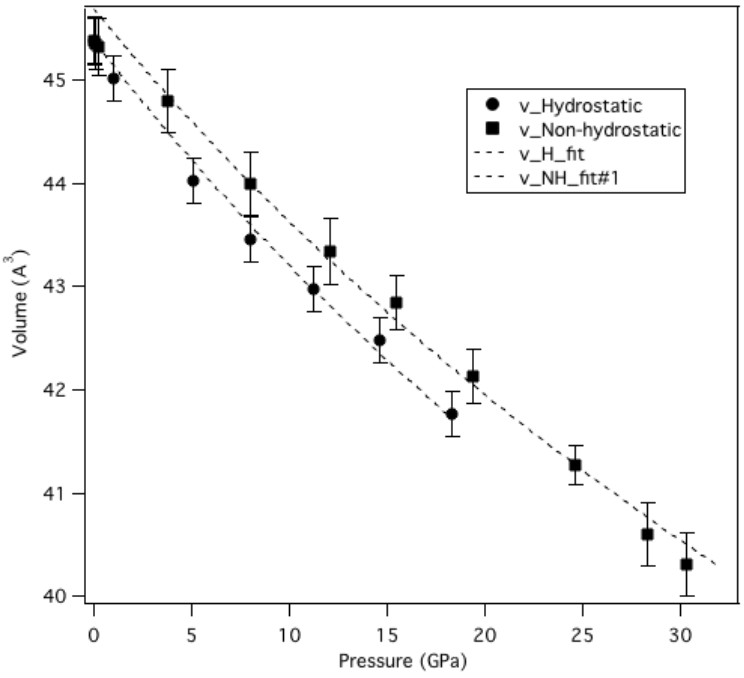

Fig. 9. Pressure vs. volume data obtained for Ni-Al-Cr under non-hydrostatic conditions is represented by solid squares. Hydrostatic data was obtained from our previous work [8] Broken lines represent their corresponding equation of state fits obtained using Birch-Murnaghan equation of state. Bulk modulus K=211.3±4 GPa was found under non-hydrostatic conditions and 166.6±5.8 GPa obtained under hydrostatic conditions for K' set as 4.

Pressure-Volume data of Ni_3Al alloyed with Cr (7.5 at %) obtained from the x-ray diffraction data collected under hydrostatic and non-hydrostatic conditions were fitted using third order Birch-Murnaghan equation of state given by,

$$P(V) = \frac{3B_0}{2}\left[\left(\frac{V_0}{V}\right)^{\frac{7}{3}} - \left(\frac{V_0}{V}\right)^{\frac{5}{3}}\right]\left\{1 + \frac{3}{4}\left(B_0' - 4\right)\left[\left(\frac{V_0}{V}\right)^{\frac{2}{3}} - 1\right]\right\}.$$

From the fit, bulk modulus and its first order pressure derivative were determined. Bulk modulus K=211.3±4 GPa was found under non-hydrostatic conditions and K=166.6±5.8 GPa obtained under hydrostatic conditions for K' set as 4.

Yield Strength (YS) is given by YS = $(\sigma_1-\sigma_3)/2$ where σ_1 and σ_3 are maximum and minimum normal stresses in axial and radial directions. According to lattice strain theory, x-ray diffraction measures strains in radial direction as the offset between hydrostatic and non hydrostatic pressures at same volume given by $2\tau/3$ with τ as the shear stress $(\sigma_1-\sigma_3)$. Shear stress of Ni-Al-Cr determined from the pressure offset measured between hydrostatic non-hydrostatic conditions at a constant volume is shown in Figure 5. A maximum shear stress of 1.8 GPa is measured at applied load of 20 GPa while the measured shear stress is found to increase linearly with applied axial load.

Yield Strength by Pressure gradient method: Pressure was measured across the Ni-Al-Cr sample loaded in a diamond anvil cell under non-hydrostatic conditions. For this experiment, Ni-Al-Cr alloy was loaded in a stainless steel sample chamber of 200 µm diameter and 50µm thickness along with few fine grain ruby crystals of <5µm distributed across the entire sample chamber. Pressure was measured by fitting the ruby florescence measured as a function of distance of the sample from the center of the sample chamber. Pressure is calibrated by the relationship of the nonhydrostatic pressure scale

$$P = 380.8[(\Delta\lambda/\lambda + 1)^5 - 1],$$

Where, λ_0 is 694.2 nm, λ is redshift in nanometers, and P is pressure in gigapascals. Figure 8 shows the various positions where the pressure was measured using ruby chips spread on the surface of Ni-Al-Cr up to 32 GPa.

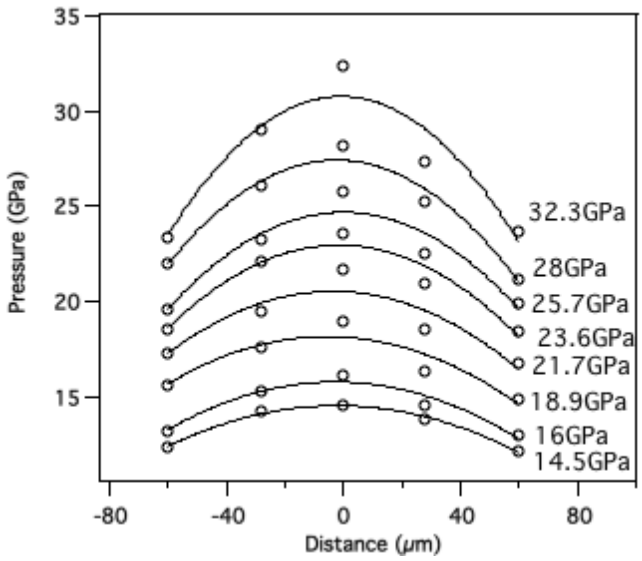

Figure 10: Mean stress distribution across the Ni-Al-Cr alloy under non-hydrostatic conditions. Pressure at each radial position across the sample is indicated by each individual point as determined by using ruby fluorescence method on the diamond sample interface. Each curve was obtained at the average sample pressure indicated.

Pressure distribution across the axially loaded sample measured under non-hydrostatic condition is shown in figure 8. Assuming sample response to be isotropic the ruby hydrostatic pressure is given by $(\sigma_1 + 2\sigma_3)/3$ which is also equal to mean normal stress. Shear stress of Ni-Al-Cr is thus obtained using the relation $t=3/2(\sigma_1- \sigma_3)$ where, σ_3 is the confining pressure and σ_1 is equal to the load stress. For pressure gradient method, Yield strength is given by YS= h/2 (dP/dr)**,** with, h the sample thickness and dP the pressure difference at a distance r from the center of the sample chamber.

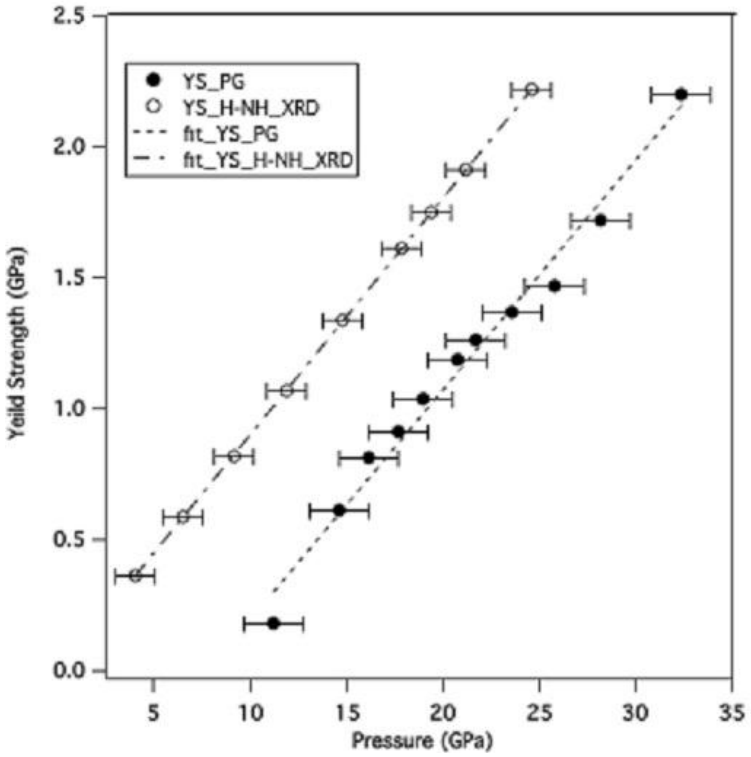

Figure 11. Comparison of yield strength determined from equation of state measurement using diamond anvil cell and by pressure gradient measurement using ruby fluorescence method.

Yield strengths estimated from pressure gradient method as a function of pressure are given in Fig. 9. It is observed that yield strength increases linearly with pressure. We estimate yield stress at 20 GPa at constant volume as offset between non hydrostatic and hydrostatic isotherms and obtain a value of about 1.8±0.3 GPa in quantitative in agreement with that obtained from pressure gradient method 1.1±0.3 GPa.

Yield strengths of Ni-Al-Cr was determined for varying load up to 30 GPa by carrying out in-situ x-ray diffraction measurements under hydrostatic and non hydrostatic conditions in the diamond anvil cell and up to 35 GPa using pressure gradient method. Both the methods show linear response for yield strength with increasing pressure. Bei et al., 2005[33] measured yield strength of Ni_3Al by Tensile measurement and found to be in the range of 400 to 600 MPa which is within the range of Ni-Al-Cr measured by using diamond anvil cell methods. The linear variation of the yield strength suggests possible increase in the number of defects and dislocations similar to the severe plastic deformation increasing the strength of the material. From the results, we can expect a change in slope is possible when there is a phase change or plastic deformation induced by the increase in the defects and dislocations. Further work on yield strength measurements under high pressure at the point of phase transformation in known alloy would provide more insight on understanding their mechanisms.

Microhardness of Ni-Al-Cr alloyed with Zr suggested from Informatics

Trace quantities of Rare-Earth additions in Ni based superalloys are known to enhance the strength of superalloys significantly [Kuang-Di Xu et al., Rare. Met. 2014]. In the search of improved non-Rare Earth superalloys, In order to compare the RE and non-RE with respect to microhardness, we have chosen the following systems 1. Ni3Al with Ce additions 0.05, 0.1, 0.15 and 0.2 at % and 2. Ni-Al-Cr with Zr additions with concentrations 0.05, 0.5, 1, and 1.5 at%. Micro Hardness of Ni_3Al with Ce addition increases from 0.05 at% up to 0.15 at% and thereafter hardness is found to decrease for 0.2 at%. In case of Zr addition from 0.05 to 1.5 at%, No significant changes in hardness was observed. The data from Vickers hardness test clearly shows addition of Zr in Ni-Al-Cr alloy has greater hardness when compared to Ni-Al-Ce alloy. Possible reason for the observed hardness change with chemical composition with respect to phase analysis and microstructure are discussed.

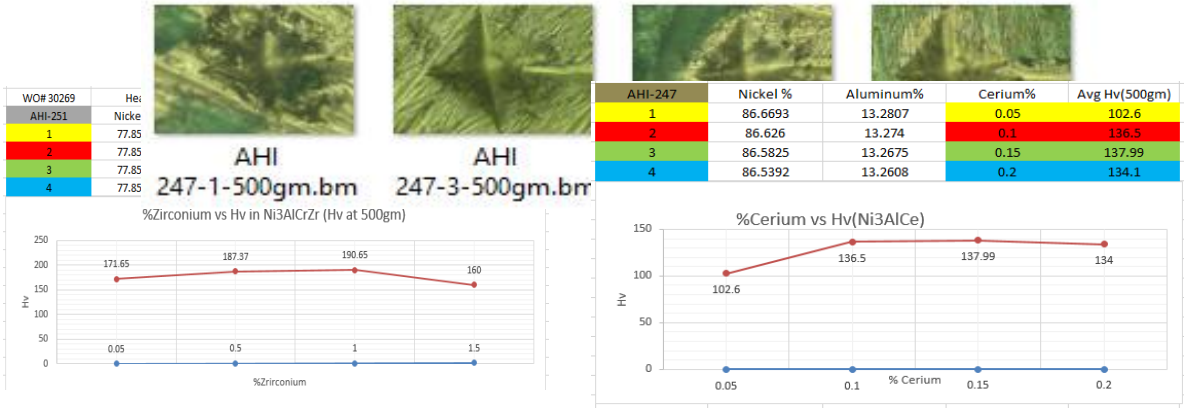

AHI-247	Nickel %	Aluminum%	Cerium%	Avg Hv(500gm)
1	86.6693	13.2807	0.05	102.6
2	86.626	13.274	0.1	136.5
3	86.5825	13.2675	0.15	137.99
4	86.5392	13.2608	0.2	134.1

Fig. 12: Tensile test provide useful and important information on strength to decide its suitability for engineering applications. We have carried out tensile measurements on Ni-Al-Co-Ti system with varying Cobalt concentration in order to compare the effect of strength on varying Co concentration. Load versus displacement was obtained and the yield strength is determined. Yield strength is found to increase with increasing cobalt content.

Sample	Thickness	Width	Cross Sectional Area	Max Load	Stress
	(mm)	(mm)	(mm2)	(N)	(N/mm2)
B1	0.46	3.00	1.38	344.16	249.39
B2	0.42	3.00	1.26	128.83	102.25
C1	0.45	3.01	1.35	235.73	174.04
C2	0.46	3.00	1.38	435.26	315.40
C3	0.44	3.00	1.32	431.47	326.87
E1	0.44	2.99	1.32	707.82	538.02
E2(b)	0.45	2.92	1.31	704.84	536.41
E3	0.46	3.00	1.38	1166.46	845.26

In the γ' phase, the $L1_2$–ordered structure consists of two sublattices, the Ni sublattice or A-site corresponding to the face-centered position and the Al sublattice or B-site corresponding to the corner position of the cubic unit cell. A common approach to predicting the site preference behavior of elements in Ni_3Al was derived from the direction of the solubility lobe of the $L1_2$–Ni_3Al phase in the ternary phase diagram [Guard]. Further, First–principles calculations have been extensively utilized to study the site preference behavior of ternary alloying elements in $L1_2$–Ni_3Al at 0 k and elevated temperatures by calculating the defect formation energies [Jiang, Jiang, Ruban, Ruban]. From first–principles calculations, it was observed that most transition metals exhibited a strong Al-site preference, with very few showing a weak Ni–site preference [Ruabn, Wu]. However, the site preference for some transition metals in $L1_2$–Ni_3Al, for example, Co was found to be composition and temperature dependent [Jiang, Ruban, Wu].

2.2.3. Microscopy Thrust

To explore the structure chemistry in the $L1_2$ phase at the atomic scale, atomic resolution STEM–EDS analysis was performed on the TEM specimen. HAADF image, Ni–Kα, Co–Kα, Al–Kα and Ti–Kα EDS maps collected from the γ′ precipitate in the <100> projection for 15Co, 30Co and 55Co are displayed in Figure #. EDS maps were acquired from the center of γ′ precipitates to avoid the compositional gradient at the γ′/γ interfaces, with sample thickness ranging between 20–30 nm for all analyzed areas. For all alloys, it is evident that Al and Ti preferentially occupy the B-sites, and Ni preferentially occupies the A-site. In Figure 13(a), the site preference of Co is not directly observable for alloy A. It is worth noting that despite the relatively low concentration of Co in the γ′ phase of this alloy, the total counts of Co sub lattice position signal detected is roughly the same as that for Ti in the same region. In other words, the Co counts collected were sufficient to resolve the Co at atomic resolution.

The signal–to–noise ratio (S/N) in the chemical maps can be enhanced by lattice averaging each map, thereby aiding direct visualization of the site preference. Lattice-averaged EDS maps acquired by averaging over eight positions are displayed in the inset for each map. Co site preference for Ni–sites is visually observed in the lattice-averaged maps in alloy B and C, while that in alloy A is not particularly convincing.

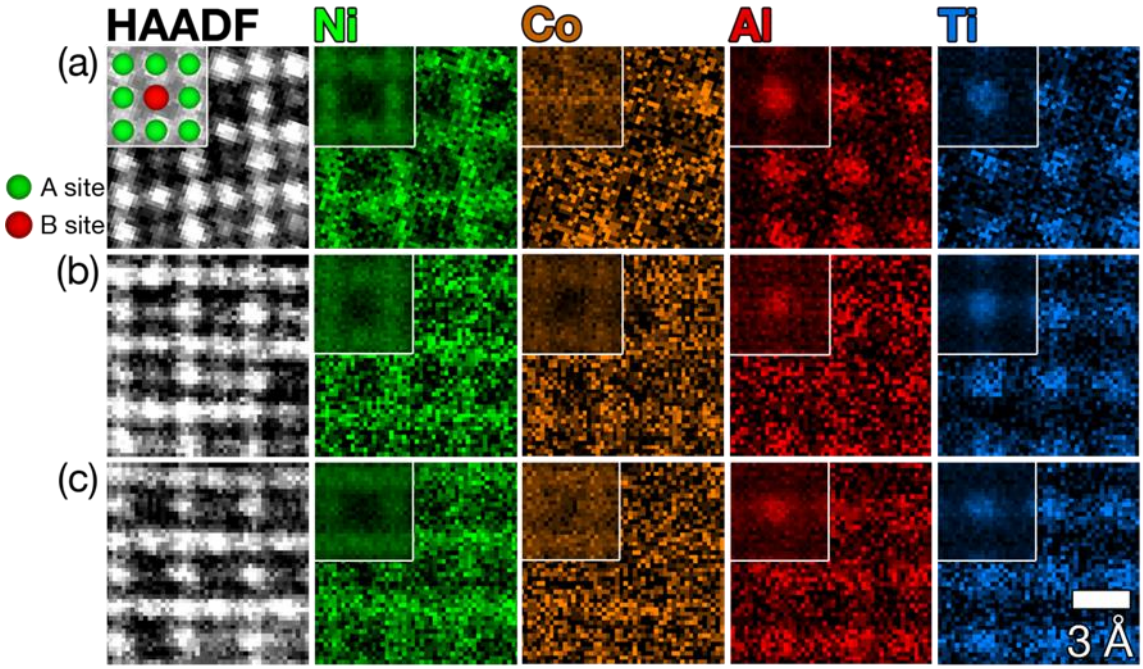

Fig. 13: Experimental EDS maps for the <001> direction of the γ′ phase in (a) 15Co. (b) 30Co and (c) 55Co. Insets shows lattice-averaged maps with enhanced S/N ratio to enable direct visualization of the site preference.

Atomic resolution EDS maps was simulated to demonstrate the effect of interatomic spacing of like atoms on EDS signal. Simulated EDS maps for randomly substituted Co on A– and B–site, and Co exclusively substituted on A–sites are presented in Figure 14(a) and (b), respectively. Substituting Co to both A– and B–sites reduces the interatomic spacing of Co, as a result, Co signal appears noisy because of signal overlap, thereby, hindering direct observation of site preference. To further explore the site preference of Co in the experimental results, qualitative comparison is made between experimental and simulated EDS maps using concentration profiles.

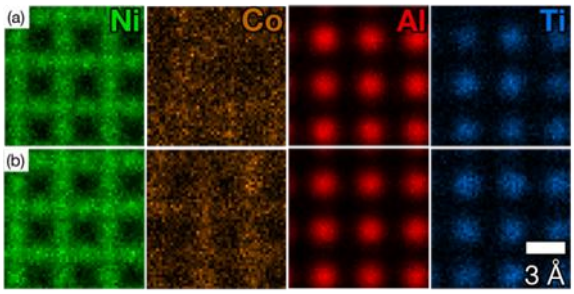

Fig. 14: Simulated EDS maps of the γ'–$L1_2$ structure when (a) Co is randomly substituted on the A- and B-sites. (b) Co is exclusively occupying the A-sites.

For both experimental and simulated EDS maps, the averaged-maps were replicated and concentration profiles are generated across the entire image. Each EDS signal was normalized and plotted over two unit cells. Concentration profiles for alloy A and simulated maps when Co is substituted on both A– and B– sites is presented in Figure 15(a). The two distinct peaks in the profiles are A, corresponding to only the A–site atoms, and B, corresponding to both A- and B-sites, as schematically illustrated in the figure. Ni signals maximize at A∗, while Ti and Al maximize at B for all alloys. The concentration profile for alloy A appears random across the entire plot, indicative that Co does not have a site preference, that is, the atoms are randomly substituted to both sites. Overall, Ni, Al, and Ti signals are in excellent agreement for both experimental and simulated data. Concentration profiles for alloy B, alloy C and simulated EDS maps when Co substituted exclusively for Ni–atoms are presented in Figure 15(b). All Co signal maximize at A∗, confirming that the Co atoms in alloy B and C preferentially occupy the Ni–sites. Results from the simulated EDS maps further substantiates our postulation that the site preference of Co changes from a random substitution for A– and B– sites at low concentration of Co to A–site preference at higher Co concentrations.

One possible explanation for the change in site preference behavior is that the co–alloying elements adapt a non–clustering trend i.e. Co exhibits a stronger Ni–site preference as the Ti concentration increases so that they are far from each other. In order to further comprehend the thermodynamic driving force for the site preference behavior observed, a combination of sophisticated computational tools capable of factoring in the sample thermal history and experimentally determined chemical

composition. Particularly, because it is challenging to accurately determine the site preference of solute atom in multi-component alloying systems using only the current first–principles calculations packages.

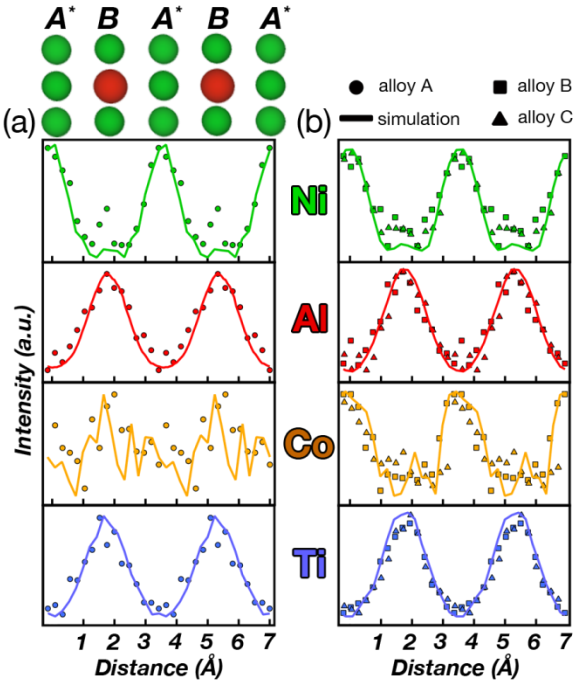

Figure 15: EDS concentration profiles from (a) 15Co and simulation with random distribution of Co. (b) 30Co, 55Co and simulation with Co fixed on A–sites.

Direct correlation between local lattice distortion and local chemistry in intermetallic alloys by Scanning Transmission Electron Microscopy

As solute atoms are added to intermetallic compounds, local chemically induced pressure develops and results in atomic displacements. These distortions play a critical role in defining the mechanical behavior of these materials, for example, by impeding dislocation motion. To investigate the correlation between the atom column chemistry and lattice distortion observed in Ni-based superalloy intermetallic compounds (γ' phase), we would be using a combination of distortion-free RevSTEM images and density functional theory (DFT) calculations. We would be analyzing the γ' precipitates in Ni-Al-Cr superalloy, which adopts the $L1_2$ structure. The main purpose of this work is to correlate local lattice distortion with local chemistry fluctuation in the projected RevSTEM images.

Fluctuation in the Al-site column intensities, seen in Figure 16(a) is a result of random variation in the local column chemistry, i.e. some columns exhibit higher Cr concentration than others. In the γ' phase, Cr atoms preferentially occupy the Al sublattice, as shown in the atomic resolution EDS map in Figure

16(b). Using atom column indexing (ACI) technique, the atom column distances are measured and projected into a matrix representation [Sang_ACI]. In Figure 16(c), each Al column is outlines by the average second line-neighbors (SLN) Ni-Ni displacement with the average displacement with the extreme contraction and expansion colored as blue or red, respectively. From visual inspection, there is some contraction (blue) around Cr-rich columns while the Al-rich columns exhibit expansion (red). A plot of the average Ni-Ni SLN distances around each Al column versus the opposing atom column (Al sublattice) is shown in Figure 20(d). The average Ni-Ni distance shows a moderate correlation with the Al sublattice column intensities. The standard deviations (σ) for the Ni-Ni nearest like neighbors (red circles) are considerably higher than those of the Al-Al nearest like neighbors (blue squares), as shown in Figure 20(e). The trend of the standard deviation for the two sublattices is suggestive of the presence of a correlated atomic distortion within the γ'phase of the Ni-Al-Cr superalloy.

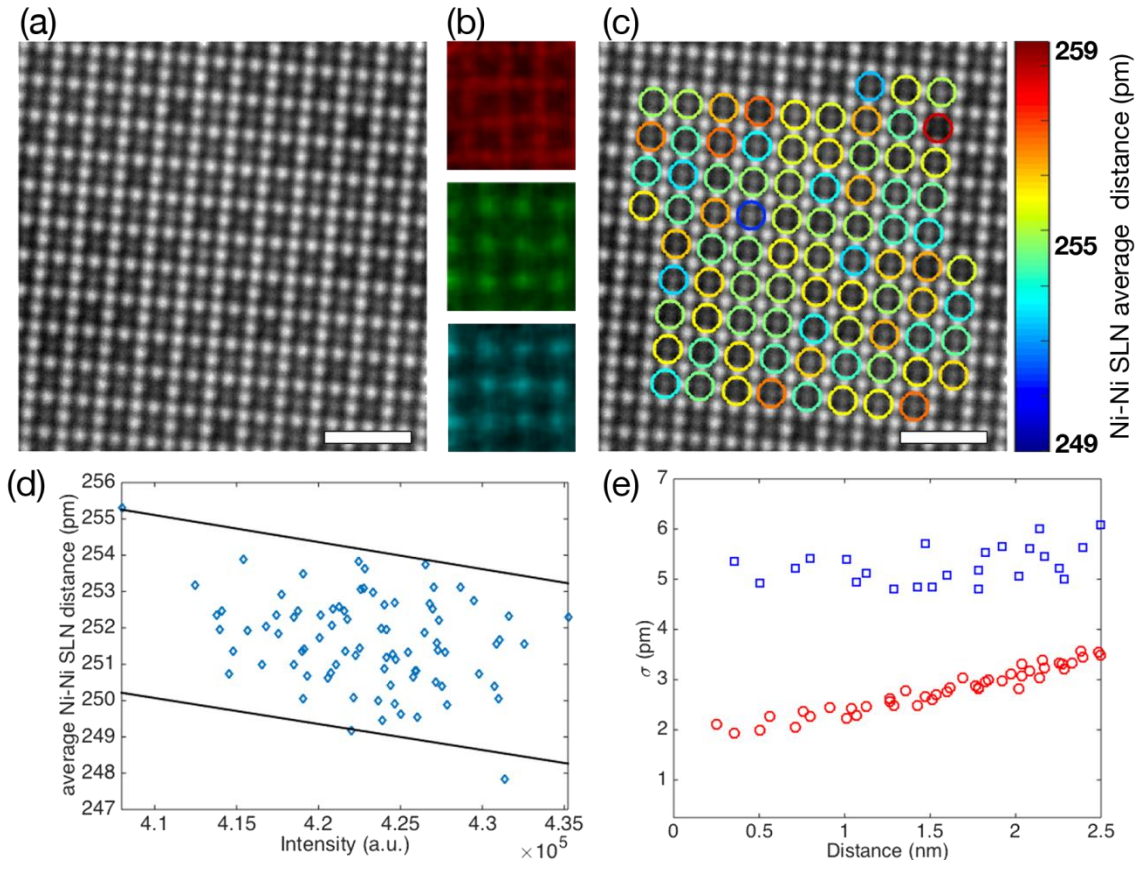

Figure 16: (a) RevSTEM image of the γ' phase in Ni-Al-Cr superalloy. (b) Atomic resolution EDS maps showing the site preference of Cr (blue) to Al (green) sublattice. (c) Average Ni-Ni second like-neighbor (SLN) distance around each Al sublattice atom column. The indicated scale bars represent 1 nm. (d) Average Ni-Ni SLN distance versus the intensity of the opposing Al atom column. (e) Standard deviation of the atom column pair distances for Ni (red) and Al (blue) sub-lattices.

To provide further evidence of the preservation of projective structural distortions in atomic resolution images, STEM images were simulated using supercells consisting of randomly distributed Cr atoms, and subsequently implementing static displacement derived from relaxed DFT supercells. The maximum static displacement of a nearest neighbor Ni atom as a result of a substituted Cr is ~2.3 pm. In addition, the 12 nearest neighbor Ni exhibited a relative contraction towards the Cr as schematically depicted in Figure 17(a). This relative contraction is probably an atom-size effect, since the atomic radius of Cr (r ~ 127 pm) is approximately 13% smaller than Al (r ~ 143 pm). Simulated STEM images with outlined lattice displacement on the Al sublattice for pure Ni_3Al and $Ni_3(Al,Cr)$ supercells are presented in Figure 21(b). A plot of the average Ni-Ni lattice distance for the two supercells as a function of the opposing Al column intensities indicates there is a correlation between the lattice displacement and local chemistry.

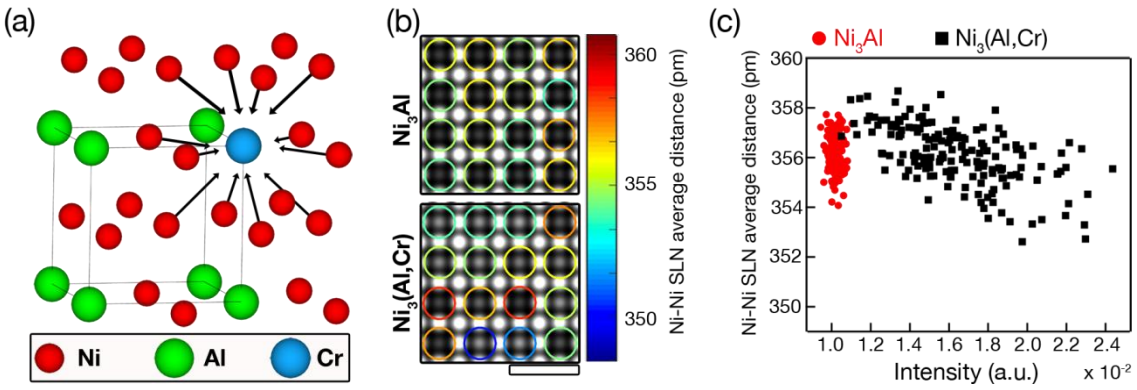

Figure 17: (a) Schematic illustration of the relative contraction of nearest neighbor Ni atoms when Cr is substituted into the Al sublattice. (b) Average SLN distances highlighted on simulated pure and alloys Ni_3Al STEM images and (c) the corresponding plot of the average Ni-Ni SLN distances as a function of Al sublattice atom column intensities.

II. RE free solute design for new Co based superalloys

2.1. Informatics Design

The ability of our graph network for capturing similarity of elements is shown in Figure 18, with the comparison between our graph network and the periodic table shown. For multicomponent systems, we have more than doubled the number of chemical additions with known behavior, for both structural stability and oxidation response. By defining the role of these elements and developing a chemical selection graph, we can now design complex multicomponent systems with targeted high temperature behavior while replacing rare earth elements. The visualization scheme exhibits the grouping and proximity of elements based on their impact on the properties of intermetallic alloys. Unlike the periodic table however, the distance between neighboring elements uncovers relationships in a complex high dimensional information space that would not have been easily seen otherwise.

This work identifies possible compositions for intermetallic formation. The nodes of the graph identify potential alloying additions and thus target the chemistries for which thermodynamic calculations need to be done to confirm whether these compounds do indeed exist. Hence the manifold learning methods serve as a screening procedure for where detailed first principles calculations need to be focused, rather than run thousands of calculations of numerous permutations of compositions and then apply machine learning algorithms to search for potential minimum energy structures. Further, while we find W to be a suitable addition, we find additional nodes that look to be as promising, such as Ta and Re. However, a single design requirement is not sufficient for identifying additives, thereby requiring multiple design pathways. For example, we have shown different pathways leading to W or to Ta, depending on the design requirement. Therefore, this identifies that a combination of these additives leads to a good combination of cohesive energy (or the highly correlated melting temperature) and modulus. This demonstrates the application of the graph network for multi-functional design.

Also identified are additional possible substitutes for quaternary systems (i.e. $Co_3(Al,X,Y)$). For instance, Ta addition to quaternary $Co_3(Al,W,Y)$ has indeed been experimentally reported [28]. We identify the new quaternary systems by including the additives which are nearest neighbors. These are further the most suitable additions to Co_3Al. This therefore guides the next series of experiments. In addition to the experiments suggested from our ternary pathways (for example, comparing the stability and melting temperature of $Co_3(Al,W)$ with $Co_3(Al,Ta)$), the melting temperature and stability should be experimentally measured. The likelihood of these compositions of intermetallics having long range order is based on the nature of similarity as characterized through manifold learning metrics. We have shown that independent studies via first principles methods that empirically explored numerous compositions do indeed match our results via informatics methods, lending support to our approach. This work has accelerated the design of RE free Co-base superalloys (Figure 19).

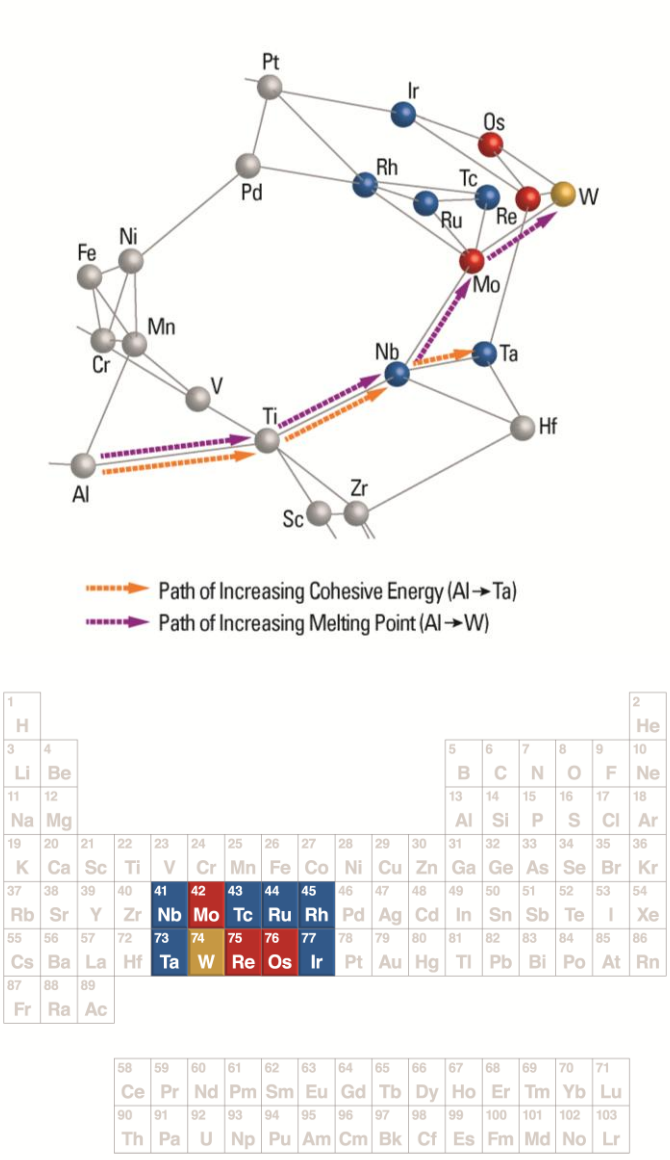

Fig. 18: Comparison of manifold representation of relative relationships of alloying elements with respect to equivalent positions as shown in the periodic table. The pathway for exploring other elements is not easily discernible looking at traditional systematics of the periodic table (for example rows, groups, Mendeleev number). The color coding is the figure serves to highlight the comparison with W addition, which is known to result in stable Co_3Al. Therefore, W is shown in gold in both the graph and periodic table, while first nearest neighbors to W are shown in red, and second nearest neighbors to W are shown in blue. From this figure, we identify multiple multicomponent RE free Co alloys.

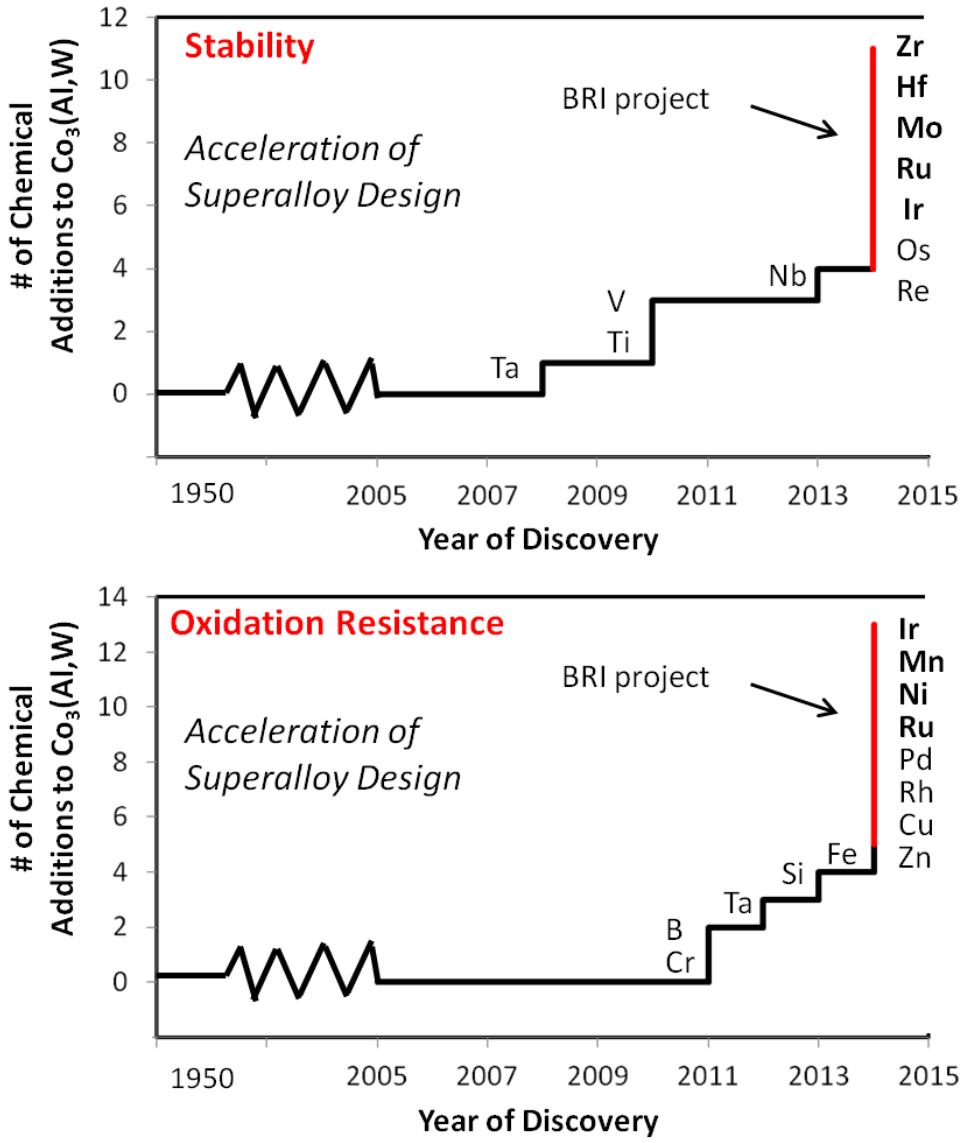

Fig 19: Accelerated discovery of Co alloy chemical substitutions (compounds in bold have empirical measurements for other characteristics). In this reporting period, we have more than doubled the number of potential elements identified as potential new L12 Co3(Al,X) intermetallics.

2.2. Mechanical Properties of Co-Based Superalloys

Cobalt based alloys have attracted broad attention due to their positive temperature dependence of strength and creep resistance better than commercial Ni based super alloys for the last 50 years. However, finding the stable $L1_2$ structured Co alloys were challenging. James et al 2011 [Advanced Materials Research Vol. 278 (2011) pp 399-404.] had recently reported a wide range of composition variation in the Ni-Al-Co-Ti system with L12 structure. However, there is no data available on the structural stability and mechanical properties of this system. we have synthesized Ni(70at%)-Al(15at%)-Co(12.35 at%)-Ti(2,65%) by arc melting followed by annealing. The microstructure and X-ray diffraction confirms the formation of the cuboids with space group Pm-3m ($L1_2$ type) structure in the Fm3m matrix. In the present work, the crystal structure stability at high pressures up to 20 GPa studied using in-situ laser heating technique will be presented. Synthesized Co-Ni-Ti-Al alloy by arc melting and heat treated fat 1000C for 3 days. X-ray diffraction confirms single phase with cubic structure. SEM and EDS Characterization - confirms cuboids formation in all the alloys.

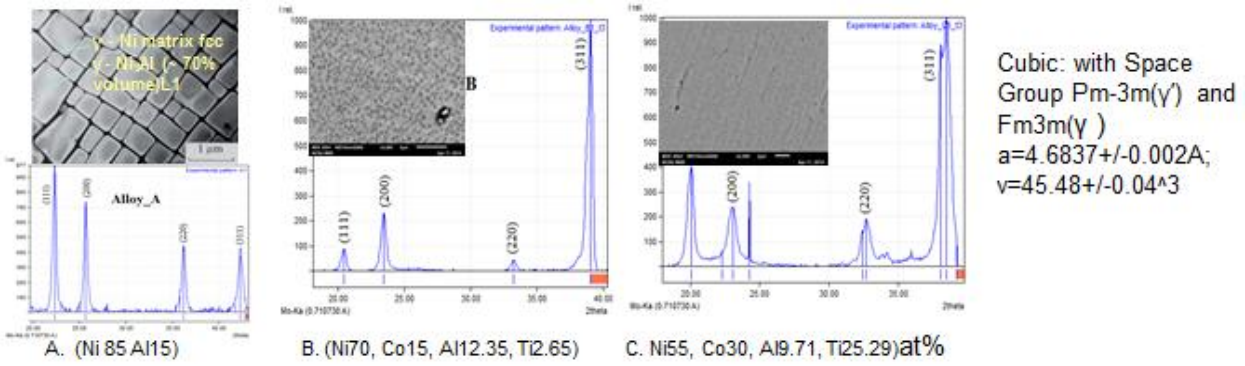

Figure 20. Synthesized Co-Ni-Ti-Al alloy by arc melting and heat treated fat 1000C for 3 days. X-ray diffraction confirms single phase with cubic structure. SEM and EDS Characterization - confirms cuboids formation in all the alloys.

Bulk modulus under hydrostatic conditions: *In-situ* x-ray diffraction (XRD) studies on Ni-Al-Co-Ti (Alloy-B) under high pressure up to 15GPa using diamond anvil cell. Ruby fluorescence was used for pressure measurement. Methal: Ethanol in the ratio 4:1 was loaded with the 10 µm sample foil served as pressure transmitting medium. The raw data and the pressure – volume data are shown below. P-V fit was obtained using third order Birch-Murnaghan isothermal equation of state is given by,

$$P(V) = \frac{3B_0}{2}\left[\left(\frac{V_0}{V}\right)^{\frac{7}{3}} - \left(\frac{V_0}{V}\right)^{\frac{5}{3}}\right]\left\{1 + \frac{3}{4}(B_0' - 4)\left[\left(\frac{V_0}{V}\right)^{\frac{2}{3}} - 1\right]\right\}.$$

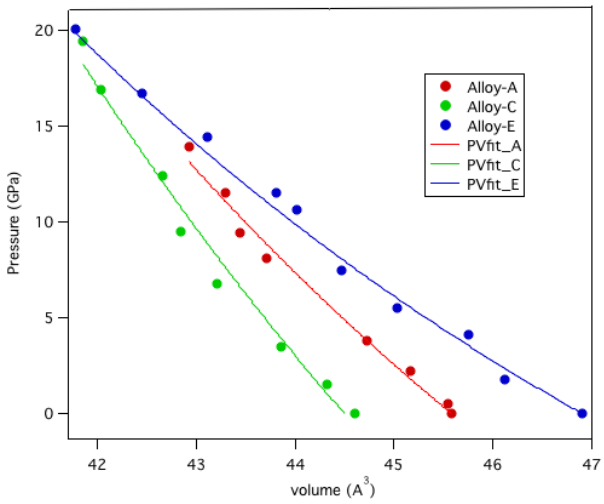

Bulk modulus		
Alloy	**K_0(GPa)**	**error**
A	194.1217	5.1374
C	263.3648	7.2899
E	136.226	5.8362

Fig 21: Extraction of bulk modulus from pressure vs. volume plot for Alloy A, C and E.. The continuous line shows fit obtained using third order Birch-Murnaghan equation of state.

Known effects Co and Ti in Ni-base superalloys: :Ti increases the volume fraction and solvus temperature of L12 phase (γ') and acts as a solid solution strengthener. Co increases the volume fraction of the $L1_2$ by reducing solubility of $L1_2$ forming elements.Al and Ti in the A1 matrix phase (γ), acts as solid solution strengthener of γ and Increases creep resistance through reduction of stacking fault energy (SFE).

ELASTIC STRENGTH AND PHASE STABILITY AT HiGH P-T CONDITIONS:

In-situ X-ray diffraction experiments were carried out at HPCAT beamline 16IDB using double sided laser heating facility up to 30 GPa and 2000C. A rhenium gasket with 30µm thickness and 100µm placed between 300 µm size diamonds served as sample chamber. Al2O3 balls of 5µm size was used to isolate the sample from touching the diamond. Alloy made into a thin foil of <10 µm thickness was loaded along with 5 µm thick MgO plate on the top. Neon was loaded along with ruby balls in the sample chamber. Pressure was measured using ruby. Three experiment runs were carried out at pressures around 5, 10, 20 and 30GPa.

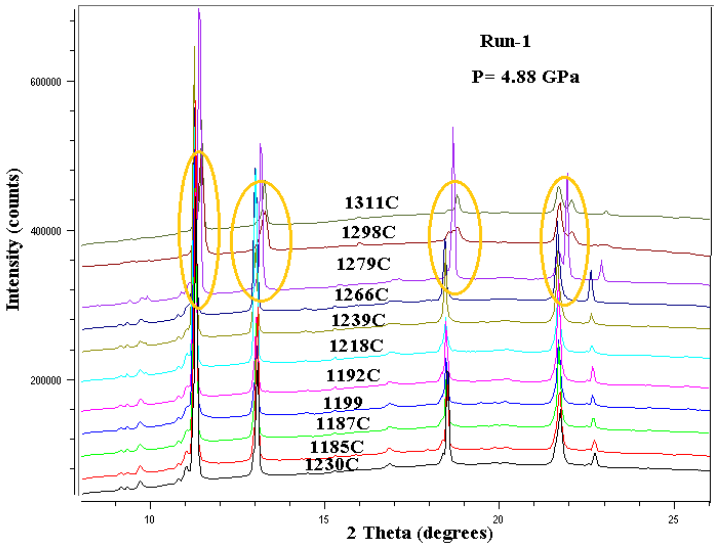

Fig. 22: XRD data collected a various temperatures during laser heating at 4.88GPaa. It can be noted that (220) And (311) peaks split while the (111) and (200) peaks overlaps. We find that Co3Ti has a larger lattice spacing than the Ni3Al.

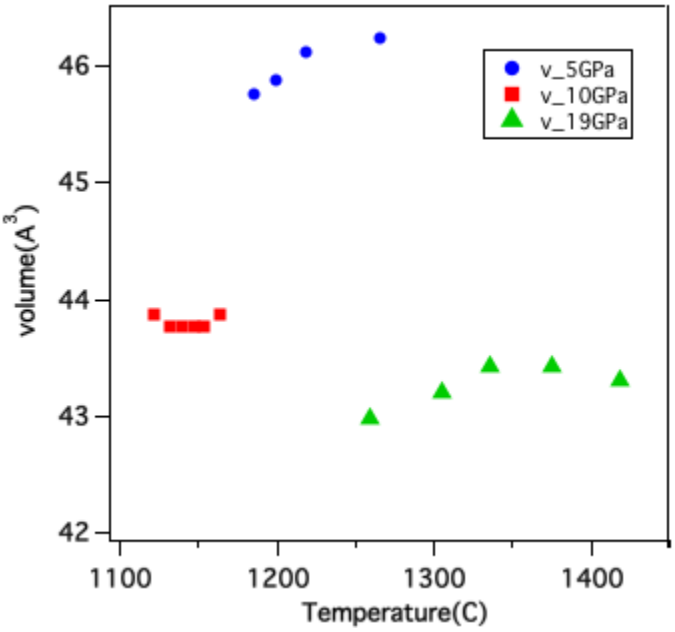

Fig. 23: Volume vs. Temperature at pressure steps of Ni-Al-Co-Ti Alloy 5GPa, 10GPa and 19GPa.

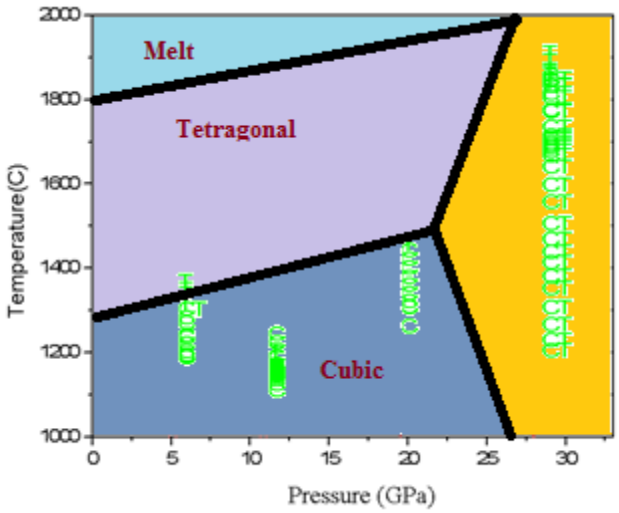

Fig 24. Phase diagram in the range up to 30 GPa and 2000 C determined from in-situ XRD using laser heating technique.

Co_3Ti and Ni_3Al phases are found to co-exists up to the highest pressure studied. Bulk modulus was found to be ~263.3+/-0.5 GPa with first order pressure derivative set to 4, which is higher than pure ordered Ni_3Al alloys.Lattice misfit between Co3Ti and Ni_3Al phases is found to increase with increasing temperature.At highest temperatures structural distortion to tetragonal phase similar to $D0_{23}$ type structure was observed. EOS fit at high temperature in progress. Phase diagram of Ni-Al-Co-Ti system is determined in the range up to maximum of 30GPa and 2000C using double sided laser heating.

IV. New high temperature intermetallics.

4.1. Informatics Based Design of RE-free Alloys

Based on the results of the Co-base and Ni-base networks, we have identified 29 Co-base and Ni-base alloys (Table 2) which are predicted to provide high temperature strength and oxidation and high temperature stability. These alloys are based on defining similarity to RE, while encompassing elements in both oxidation pathways and stability pathways. We have limited our selection to quaternary systems at this point, but the approach and networks are expandable to more complex alloy chemistries. Further, we have limited this selection to elements that are nearest neighbors of RE elements and also next nearest neighbors. The selection of alloys through this logic is confirmed as all combinations identified by this approach which have also been previously reported have been proven to exist. Further, none of the alloys identified have been negatively reported in the literature. This table therefore provides a significantly reduced search space, making the identification of the best RE free alloy manageable. As a starting point and for developing the integrated thrusts, we have selected Ni-Co-Al-Ti for further analysis. The correlative results from this informatics selected alloy are discussed throughout this report, as analyzed by a variety of approaches.

Table 2: RE-free alloys identified through the use of informatics design, following the Figs. 2 and 18. Through this work, we have reduced the alloy search space to these 29 alloys.

RE-free Co-Base Alloys	***RE-free Ni-Base Alloys***
Co-Ni-Al-Ti	Ni-Al-Hf-Zr
Co-Ni-Al-Ta	Ni-Al-Hf-Ti
Co-Ni-Al-Nb	Ni-Al-Zr-Ti
Co-Ni-Al-Mo	Ni-Al-Zr-V
Co-Ni-Al-V	Ni-Al-Zr-Nb
Co-Al-W-Re	Ni-Al-Hf-V
Co-Al-W-Os	Ni-Al-Hf-Nb
Co-Al-Mo-Rh	Ni-Al-Ti-Nb
Co-Al-Re-Ta	Ni-Al-Nb-Ta
Co-Al-Mo-Ru	Ni-Al-Ti-V
Co-Al-Re-Os	Ni-Al-Nb-Mo
Co-Al-Re-Ir	Ni-Al-V-Cr
Co-Al-Mo-Nb	Ni-Al-V-Ta
Co-Ni-Al-Re	Ni-Al-V-Mo
Co-Al-Re-Os	

4.2. Search of $L1_2$ systems in other high melting alloys using thermodynamic approach

We have searched the formation of $L1_2$ systems in the super alloys (Ni_3Al, Co_3Ti). There may be compositional regions in the quadrilateral with complete miscibility. Therefore a systematic study of the ternary and quartenary alloys is required. The strategy adopted is to search for compositions that yield predominantly the two phase fields with $L1_2$ and FCC phases. We may pick alloy compositions along the

plane with corners Ni_3Al-Co_3Ti but thermodynamically there are 4 ternary systems. We have studied all the ternary syatems using the available data in the Factsage and SpMBCN databases and found compositional regions for the coexistence of the ordered and disordered phases. These areas are further studied by adding a 4th element. The paper describing this is;

Since the two-phase texture (FCC_L12 and FCC) has been shown to have increased strength, it is interesting to examine the phase relation changes when a 4th element is added. We chose several points in the grey area (Al:Ni:Ti). To these compositions 1 mole of C was added and phase equilibrium was calculated The calculations indicate that the single phase area became a two or three-phase area by addition of carbon with most carbon included in the FCC phase.

Table 3.Wt% of elements in the alloys.

Phases							
FCC_L12	Liquid	FCC_A1	T melt K	Al	Ni	Ti	C
5.45	3.32	1.22	1590	5.81	33.49	59.41	1.29
8.54	0	1.45	1371	7.71	8.05	83.23	0.99
8.32	0	1.71	1402	2.4	10.15	86.63	0.82
4.42	4.2	1.39	1300	8.6	24.95	65.16	1.27

Most of the carbon is accommodated in FCC phase and therefore by varying the carbon content, we can vary the proportions of the two phases and change the physical properties of our alloy. A second ternary in this system could be Ti-Ni-Co. Considering that Al inclusion may result in lower melting temperature for the alloy, we have considered the three more refractory elements of the quaternary system. The composition field of interest is shown in Fig. 24 we have synthesized the compositions in table 3 and characterization analysis is in progress.

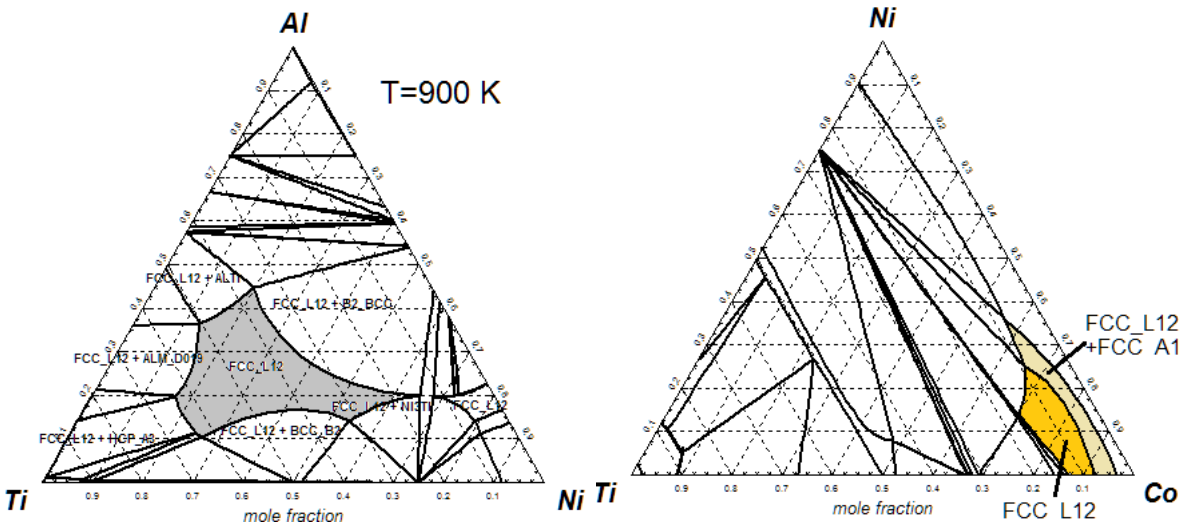

Fig. 25. The Ni-Ti-Co ternary at 1100 K

V. Informatics guided DFT based simulations of "virtual alloys"; and

A method for integrating DFT calculations from UF and informatics analysis of ISU was developed for purpose of providing design rules for site substitution of alloy addition. This work accelerates the prediction of new alloy chemistries, which otherwise requires time consuming calculations. By analyzing density of states (DOS) spectra with an informatics approach, we were able to predict the site occupancy in Ni_3Al compounds by simultaneously mapping mechanical property, electronic structure, and chemistry. In this project, we have expanded this approach to incorporate a larger number of compounds (Figure 26).

Through this integration of DFT and informatics, we develop design rules for selection of additives based on site occupancy. The input into the analysis is the DOS spectra when replacing a Ni or Al atom. By tracking the change in this map with increasing substitute composition, we identify the energetically preferred site. We identify Ce as occupying either site, while all others have a preferred site. This work accelerates the design of new Ni-based alloys by screening for possible chemistries without requiring additional calculations on chemical energy changes.

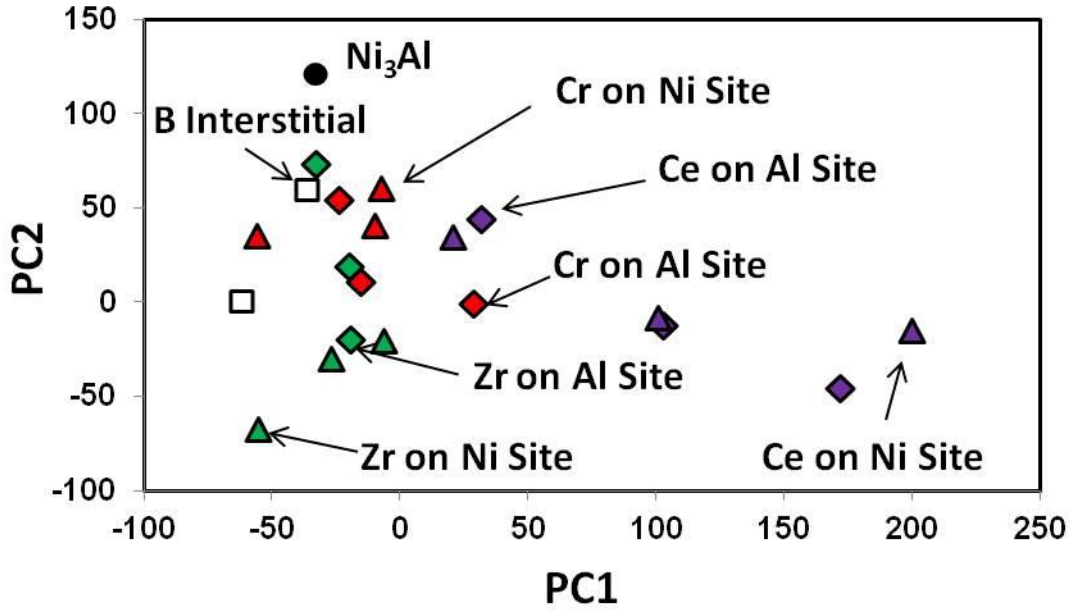

Fig. 26. Mapping of chemical site preference, with the trajectory defining the site occupancy. When adding further additives moves the point further from Ni_3Al point, then that is energetically favorable. Ce is the only element here which occupies either site, with all others having a preferred site. Diamond is substitute on Al site, triangle is substitute on Ni site, and square is interstitial site occupancy.

VI. STEM / Atom Probe correlative microscopy.

The controlled simultaneous alloying of Co and Ti with Ni-based superalloy takes advantage of the increased strength of γ'-Co_3Ti over γ'-Ni_3Al at high temperature [Cui]. Addition of Ti to Ni-Al increases the volume fraction and solvus temperature of the $L1_2$ phase, while Co increases the creep resistance by reducing the stacking fault energy in the γ matrix [Reed, Minshull]. Furthermore, the site preference of solute atoms in the $L1_2$ structure has significant implications on the high–temperature mechanical properties, microstructural stability and resistance to chemical degradation [Reed]. Therefore, determining the effect of composition on the coherency strain and volume partitioning between γ' and γ phases, and site preference in the γ' phase is pertinent in engineering new generation of efficient superalloys for high temperature applications.

Analysis was performed on directionally solidified superalloy samples with a systematic composition matrix as adapted from Ref. [Minshull]. Nominal composition of the quaternary superalloy system examines are presented in Table 4. Solution heat treatments were performed in a quartz tube at 1330 ◦C

(15Co and 30Co) and 1245 ◦C (55Co). Subsequently, all the alloys were aged at 750 ◦C for 7 days to ensure homogeniety.

Table 4: nominal composition of the Ni-Co-Al-Ti superalloy samples (in at %).

Alloy	Ni	Co	Al	Ti
15Co	70.0	15.0	12.35	2.65
30Co	55.0	30.0	9.71	5.29
55Co	30.0	55.0	5.29	9.71

To minimize the sample volume and thus magnetic interactions with the electron beam, TEM specimen were prepared via the lift-out technique using a dual-beam focused ion beam (FIB) microscope (Quanta 3D FEG, FEI) with 30 kV Ga+, followed by 5 kV Ga+ and 2 kV Ga+ milling to reduce surface damage contamination. TEM specimen were kept under vacuum and analyzed within 48 hours after preparation to reduce oxide formation. High- angle annular dark-field (HAADF) images and EDS data shown in this study were acquired using a probe-corrected FEI Titan G2 60–300 kV S/TEM equipped with a Schottky field emission gun (X-FEG) source operated at 200 kV. The probe convergence angle α and inner collection semi-angles for HAADF imaging were 13.5 mrad and 77 mrad, respectively. Position averaged convergent beam diffraction (PACBED) patterns were used to measure the average specimen thickness for area of analysis [LeBeau-PACBED]. Revolving STEM (RevSTEM) image series contained a total of 20 1024×1024 frames, acquired with a dwell time of 2 µs/pixel [Sang_RevSTEM]. EDS maps were generated using the X-ray K-line for each element. Raw EDS data were extracted into a custom MATLab code to average the signal into a single unit cell, employing the lattice-averaging method reported by Ref. [PingLu].

Three-dimensional periodic supercell of the L12–Ni3Al structure with 10×10×140 unit cells (56000 atoms) were generated for two Co site preference conditions. The lattice parameter of the unit cell is 3.57 Å, as measured from the RevSTEM image of the γ’ phase of alloy A. The supercell compositions were designed to approximately match the APT measured composition of the $L1_2$ phase in 15Co. For the first supercell, the composition is 71.27Ni-4.875Co-18.5036Al-5.3482Ti at. %, where all the Ti were substituted to only Al sublattice, while Co was randomly substituted for Al and Ni atoms. In the second supercell, the composition is 70.01Ni-4.9875Co-19.157Al-5.8429Ti at. %, where all Ti and Co exclusively substituted the Al and Ni atoms, respectively. Atomic resolution EDS simulations were performed using the µSTEM software package [Allen2015]. The images were simulated using experimental conditions. Simulated images were convolved with a Gaussian function, 1.3 Å full-width half-max, to approximately account for the finite effective source size. Blurred maps were resampled to match the pixel size of the experimental maps. Furthermore, noise was applied to the simulated maps using a Poisson random function- taking into account the acquisition time, beam current and detector solid angle- to match the experimental EDS maps.

A representative image of the microstructure in 15Co, presented in Figure 27(a), shows the uniformly distributed cuboidal γ′ precipitates in the γ matrix. The precipitates morphology is indicative of a substantial lattice misfit between γ′- and γ-phases (>0.3%), consistent with the results reported in Ref. [Minshull]. The corresponding EDS chemical maps, presented in Figure 27(b), shows that Co is partitions to γ phase, Al and Ti partitions to γ′ precipitate, while Ni is evenly distributed between both phases.

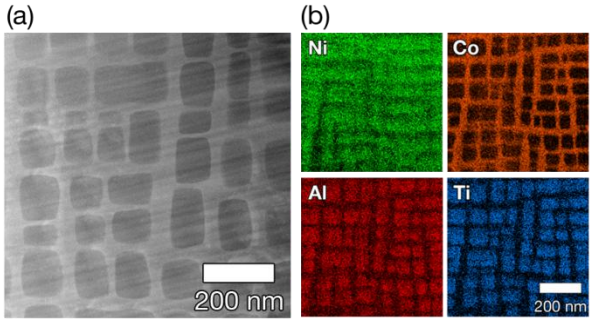

Fig. 27: (a) STEM image of the microstructure in 15Co. (b) corresponding EDS chemical maps.

The overall microstructure and chemical volume partitioning in 30Co, as seen in Figure 28(a) is similar to that of 15Co. However, Ni volume partitioning to the γ′ precipitate is higher in this sample in comparison to the previous sample.

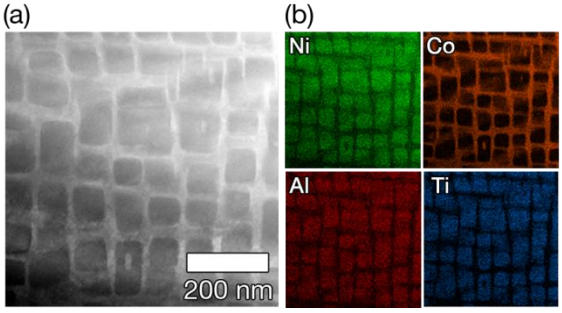

Fig. 28: (a) Microstructure of 30Co (b) corresponding EDS maps.

The relatively large lattice misfit between γ′ and γ phases in 55Co results in discontinuous coarsening (non-cuboidal precipitates) in these alloys, as shown in Figure 29(a). With increasing Co and Ti content, the lattice misfit between γ′ and γ phases increases. This is possibly as a result of the volume partitioning of Ti to the γ′ phase, leading to a positive Vegard's coefficient for the $L1_2$ phase [minshull]. The high

stacking fault density observed at the γ'/ γ interfaces in this alloy, shown in Figure 30 is an evidence of the large lattice mismatch in the alloy.

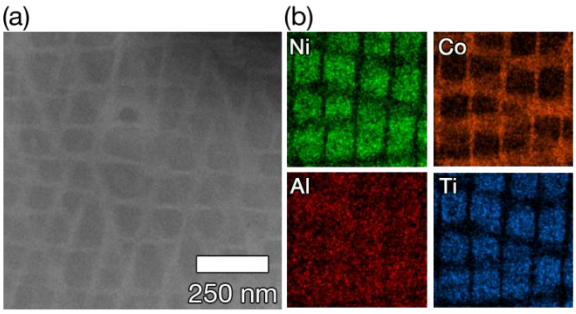

Fig. 29: (a) Microstructure of 55Co (b) corresponding EDS maps

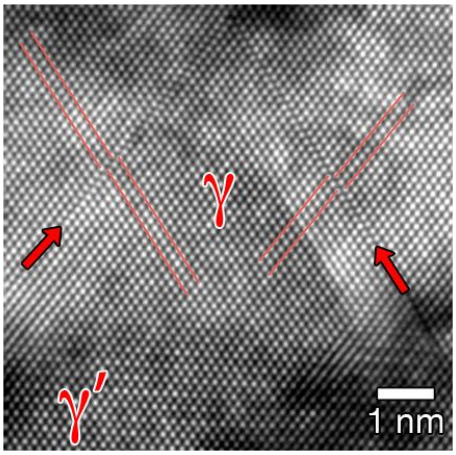

Fig. 30: RevSTEM image of the γ'/ γ interface in 55Co alloy down the <110> projection. The stacking faults (highlighted by the arrows) are a result of a relatively high lattice mismatch between the γ' and γ phases in the alloy.

The change in microstructure morphology and lattice misfit between γ' and γ with change in alloy composition necessitates an investigation of the coherency stresses between γ' and γ phases at the atomic scale. For this study, we would be utilizing the large area strain analysis technique that enables accurate strain measurement in distortion-corrected RevSTEM images [Oni2015]. The distribution of local strain within the alloy is systematically measured from the center of the γ' precipitate to the γ'/ γ' interface along two orthogonal paths, A and B. The average ε_{xx} and ε_{yy} from each image along paths A and B is presented in Figure 35(a). Along path A, ε_{xx} and ε_{yy} are perpendicular and parallel to the γ'/ γ' interface plane, respectively. With respect to the central γ' region, the strain drops suddenly within the γ

phase to ~-1.5% in the direction parallel to the interface. This relationship is reversed along path B where the large negative strain is observed for ε_{xx}.

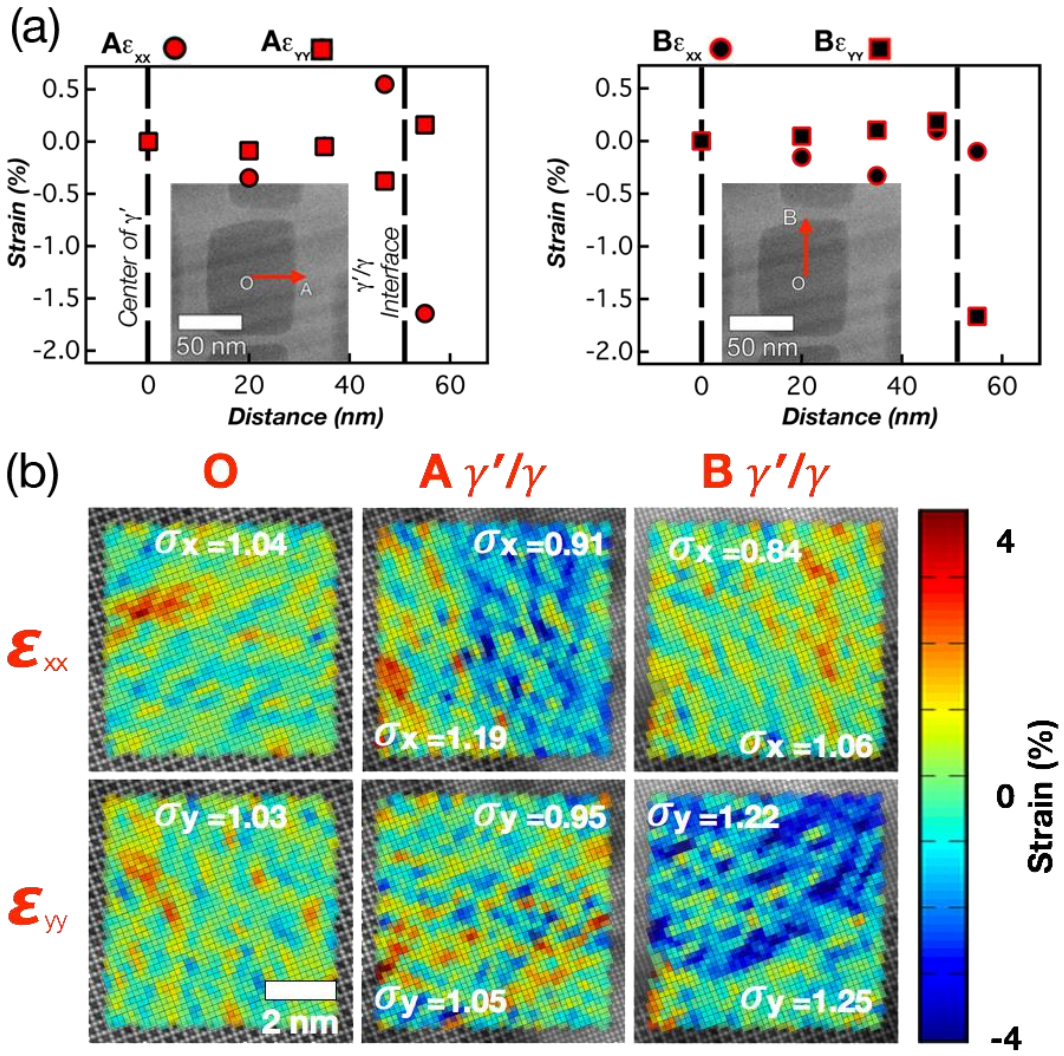

Fig. 31: (a) Average lattice strain as a function of distance to interface along paths A and B. (b) Strain maps at the center of gamma prime (O), and γ'/ γ interfaces at A and B.

Strain maps of RevSTEM images acquired at the center of the γ' precipitate (O), and the γ'/ γ interfaces along path A and B are presented in Figure 5(b). Unlike the average strain from each image plotted in Figure 32(a), the unit-cell strain measured locally at the γ'/ γ interfaces drop to as low as -4%. This is because such high compressive strain gets averaged out in the average strain, further highlighting the benefit of this real-space strain analysis technique for *local* strain measurements.

APT results: Atom probe tomography (APT) was employed to quantify the chemical composition in the alloys. Figure 32(a) presents 3D atom probe (3DAP) reconstruction of Ni atoms (green), Co atoms (orange), Al atoms (red) and Ti atoms (blue) for alloy A. The corresponding concentration profiles across the γ′/γ interface is displayed in Figure 32(b). It is apparent that Al and Ti partitions to the γ′ phase, Co partitions to the γ phase, and Ni exhibits an even distribution across both phases. Table 5 contains the measured composition in the γ′ and γ phases for 15Co, 30Co and 55Co, respectively. The partitioning ratio, $\kappa_i^{\gamma'/\gamma}$ defined as the ratio of the concentration of an element *i* in the γ′ phase to the concentration of the same element in the γ phase:

$$\kappa_i = \frac{C_i^{\gamma'}}{C_i^{\gamma}}$$

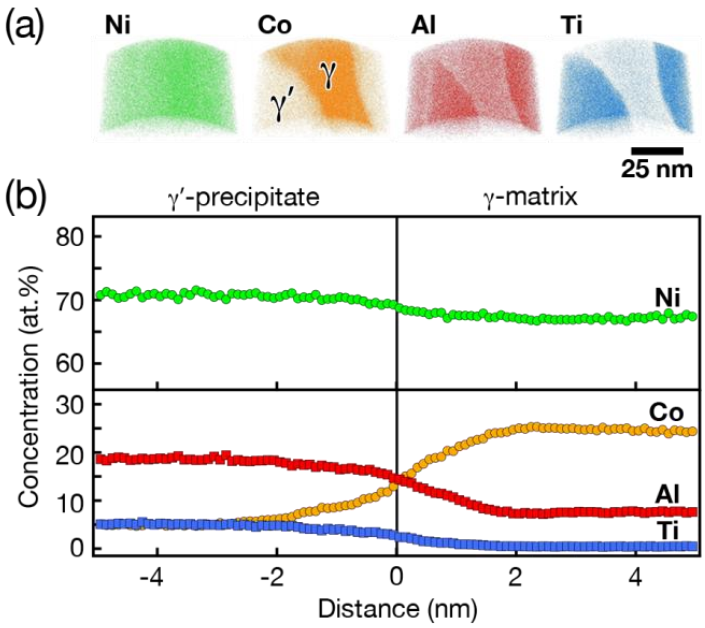

Fig. 32: (a) 3D atom probe reconstructed image of 15Co specimen. (b) Proximity histogram depicting the compositional transition across the interface.

Table 5: Atom probe tomography (APT) measured chemical composition in the γ′ and γ phases for all alloys. The calculated partition coefficients for each alloy are also presented.

Alloy	Phase	Ni	Co	Al	Ti	κ(Ni)	κ(Co)	κ(Al)	κ(Ti)
15Co	γ′	71.005	4.885	18.746	5.364	1.0525	0.1999	2.4582	11.129
	γ	67.46	24.43	7.626	0.482				
30Co	γ′	61.653	12.802	15.956	9.589	1.4968	0.2305	5.5211	21.793
	γ	41.19	55.55	2.89	0.44				
55Co	γ′	42.682	32.72	8.089	16.509	2.6112	0.4084	3.7817	11.775
	γ	16.346	80.113	2.139	1.402				

References:

T.E. Graedel, et al. *Proceedings of the National Academy of Sciences,* 12752 (2013)
C.Y. Cui, Y.F. Gu, D.H. Ping and H. Harada: Intermetallics 16 (2008) p. 910-916.
R. C. Reed, The superalloys: Fundamentals and Applications (Cambridge University Press, U.K., 2006).
J. P. Minshull, S. Neumeier, M. G. Tucker, and H. J. Stone, Advanced Materials Research 278, 399 (2011).
J. M. LeBeau, S. D. Findlay, L. J. Allen, and S. Stemmer, Ultramicroscopy 110, 118 (2010).
X. Sang and J. M. LeBeau, Ultramicroscopy 138, 28 (2014).
P. Lu, L. Zhou, M. J. Kramer, and D. J. Smith, Scientific reports 4 (2014).
L. Allen, A. DAlfonso, and S. Findlay, Ultramicroscopy 151, 11 (2015).
A. A. Oni, X. Sang, S. V. Raju, S. Dumpala, S. Broderick, A. Kumar, S. Sinnott, S. Saxena, K. Rajan, and J. M. LeBeau, Applied Physics Letters 106, 011601 (2015).
R.GuardandJ.Westbrook,TRANSACTIONSOFTHEAMERICANINSTITUTEOFMINING AND METALLURGICAL ENGINEERS 215, 807 (1959).
C. Jiang and B. Gleeson, Scripta materialia 55, 433 (2006).
C. Jiang, D. Sordelet, and B. Gleeson, Acta Materialia 54, 1147 (2006).
A. Ruban and H. Skriver, Solid State Communications 99, 813 (1996).
A. V. Ruban and H. L. Skriver, Phys. Rev. B 55, 856 (1997).
X. Sang, A. A. Oni, and J. M. LeBeau, Microscopy and Microanalysis 20, 1764 (2014).

List of Publications and Invited Presentations:

Publications:

1. Information-driven Approaches to Materials Discovery and Design Eds. T. Lookman, F. Alexander and K.Rajan: Springer Series in Materials Science (2016)
2. S.R. Broderick and K. Rajan "Discovering Electronic Signatures for Phase Stability of Intermetallics via Machine Learning" in *Information-driven Approaches to Materials Discovery and Design* Eds. T. Lookman, F. Alexander and K.Rajan: Springer Series in Materials Science, Ch. 12 (2016)
3. F Vurpillot, W.Lefebvre, J.M. Cairney, C. Oberdorfer, B.P. Geiser and K. Rajan. "Advanced volume reconstruction and data mining methods in atom probe tomography" *MRS Bulletin* 41, 46-52 (2016)
4. A. J. Zaddach, C. Niu, A. A. Oni, M. Fan, J. M. LeBeau, D. L. Irving, C. C Koch. "Structure and magnetic properties of a multi-principal element Ni-Fe-Cr-Co-Zn-Mn alloy" Intermetallics 68, 107-112 (2016)
5. O.Wodo , S. Broderick and K. Rajan, " Microstructural Informatics to Driven Rational Materials Design", *MRS Bulletin* (August 2016- in press)
6. S. Broderick and K. Rajan , ""Harnessing the BigData Paradigm for ICME: transforming from materials selection to materials enabled design" *JOM- TMS Journal of Metals, Minerals and Materials Society* (August 2016 – in press)

7. S. Srinivasan, S.R. Broderick, R. Zhang, A. Mishra, S.B. Sinnott, S.K. Saxena, J.M. LeBeau, K. Rajan. "Mapping Chemical Selection Pathways for Designing Multicomponent Alloys: An Informatics Framework for Materials Design." *Nature Scientific Reports*, 5, 17960 (2015)
8. S. Srinivasan, K. Kaluskar, S. Broderick, K. Rajan. "Extracting Features Buried within High Density Atom Probe Point Cloud Data through Simplicial Homology." *Ultramicroscopy* 159, 374-380 (2015)
9. S. Srinivasan, K. Kaluskar, R. Dumpala, S. Broderick, K. Rajan. "Automated Voxelation of 3D Atom Probe Data through Kernel Density Estimation." *Ultramicroscopy* 159, 381-386 (2015)
10. C.S. Kong, S.R. Broderick, T.E. Jones, C. Loyola, M.E. Eberhart, K. Rajan. "Mining for Elastic Constants of Intermetallics from the Charge Density Landscape." *Physica B*. 458, 1-7 (2015)
11. C. Niu, A. J. Zaddach, A. A. Oni, X. Sang, J. W. Hurt III, J. M. LeBeau, C. C. Koch, D. L. Irving, "Spin-driven Ordering of Cr in the Equiatomic High Entropy Alloy NiFeCr", Applied Physics Letters, 106, (161905) 2015
12. A. A. Oni, X. Sang, S. V. Raju, S. Dumpala, S. Broderick, A. Kumar, S. B. Sinnott, S. K. Saxena, K. Rajan, J. M. LeBeau, "Large Area Strain Analysis Using Scanning Transmission Electron Microscopy Across Multiple Images" Applied Physics Letters, 106, (011601) 2015.
13. C.S. Kong, S.R. Broderick, T.E. Jones, C. Loyola, M.E. Eberhart, K. Rajan. "Mining for Elastic Constants of Intermetallics from the Charge Density Landscape." *Physica B*. 458, 1-7 (2015)
14. S.V. Raju, A. A. Oni, B. K. Godwal, J. Yan, V. Drozd, S.Srinivasan, J. M. LeBeau, K.Rajan, S. K .Saxena,"Effect of B and Cr on elastic strength and crystal structure of Ni3Al alloys under high pressure", *J. of Alloys and Compounds* 619 (2015) 616-620 .
15. S.V. Raju, B.K. Godwal, J. Yan, R. jeanloz, S.K. Saxena, "Yield strength of Ni-Al-Cr superalloy under presuure.", *J. Alloys and Compounds* 657 (2015) 889-892.
16. A. Kumar *at al., "*Charge optimized many-body (COMB) potential for dynamical simulation of Ni–Al phases", *J. Phys. Cond. Matt.* 27, 336302 (2015)
17. A. Kumar, A. Chernatysnkiy, M. Hong, S.R. Phillpot and S.B. Sinnott, "An ab initio investigation of the effect of alloying elements on the elastic properties and magnetic behavior of Ni_3Al", *Comput. Mater. Sci.,* 101, 39-46 (2015)
18. S.V. Raju, Z. Geballe, B.K. Godwal, B. Kalkan, Q. Williams, R. Jeanloz,, "High Pressure and Temperature structure of Liquid and Solid Cd: Implications for the melting curve of Cd" *Materials Research Express* (2014) 046502
19. S.Broderick, U. Ray, S. Srinivasan, K. Rajan, G. Balasubramanian, "An Informatics Based Analysis of the Impact of Isotope Substitution on Phonon Modes in Graphene", *Applied Physics Letters* 104, 243110 (2014)
20. S. Dumpala, S.R. Broderick, P.A.J. Bagot, K. Rajan, "An Integrated High Temperature Environmental Cell for Atom Probe Tomography Studies of Gas-Surface Reactions: Instrumentation and Results", *Ultramicroscopy* 141, 16-21 (2014)
21. R. F. Zhang and K.Rajan, "Statistically Based Assessment of Formation Enthalpy for Intermetallic Compounds"; Chem.Phys. Lett. 612, 177-181 (2014)
22. Informatics for Materials Science and Engineering: editor Krishna Rajan ; Elsevier ISBN: 9780123943996 (2013)
23. S. Kalavathi, S.V. Raju, Q. Williams, P Ch Sahu, V S Sastry and H K Sahu, "Pressure-induced frustration in charge ordered spinel AlV2O4", *J. Phys.: Condens. Matter* 25 292201 (2013).

24. Z.M. Geballe, S.V. Raju, B.K. Godwal and R. Jeanloz, "Clapeyron slope reversal in the melting curve of AuGa2 at 5.5 GPa", *J. Phys.: Condens. Matter* 25 415401 (2013).
25. S.B. Sinnott, "Material Design and Discovery with Computational Materials Science", *J. Vac. Sci. Technol. A* **31**, 050812 (2013)
26. S.R. Broderick, A. Bryden, S.K. Suram, "Data Mining for Isotope Discrimination in Atom Probe Tomography." *Ultramicroscopy*, **132**, 121-128 (2013)
27. J. Peralta, S.R. Broderick, K. Rajan. "Mapping Energetics of Atom Probe Evaporation Events through First Principles Calculations." *Ultramicroscopy*, **132**, 143-151 (2013)
28. A. Bryden, S. Broderick, S.K. Suram, K. Kaluskar, R. LeSar, K. Rajan. "Interactive Visualization of APT Data at Full Fidelity." *Ultramicroscopy*, **132**, 129-135 (2013)
29. S.K. Suram, K. Rajan. "Calibration of Reconstruction Parameters in Atom Probe Tomography Using a Single Crystallographic Orientation." *Ultramicroscopy*, **132**, 136-142 (2013)
30. S.Broderick, S.Srinivasan, R. Zhang and K.Rajan: "Identification of Critical Element Substitutes for Ni Based Superalloy Design via Manifold Learning" *Proc. National Academy of Sciences (submitted)*
31. S.K. Saxena, S.V. Raju, K. Rajan, S. Broderick. "Searching L12 phase in ternary and quaternary super alloy compositions (Ni-Al-Co-Ti)" *Calphad* (submitted)
32. S.V. Raju, B. K. Godwal, S. Srikant, J. Yan, K. Rajan and S. K .Saxena, "Strain variation across lattice planes of Ni_3Al:B(500ppm) as a function of applied load". (In preparation).
33. S.V.Raju, R. Hrubiak, V.Drozd, S. K .Saxena, "Phase stability of Ni-Co-Ti-Al based $L1_2$ superalloys with varying composition of Co", Appl. Phys. Lett.*(To Submit*).
34. S.V. Raju, B. K. Godwal, J. Yan, S. K .Saxena, "Yield strength of Cr doped Ni_3Al from hydrostatic and non-hydrostatic compression", *J. Alloys and Compounds (Under Review*).
35. A. Kumar, T. Liang, A. Chernatynskiy, S.R. Phillpot and S.B. Sinnott, "Effect of defects on the strength on Ni_3Al-Al_2O_3 interfaces using Molecular Dynamics studies" (in preparation)
36. A. Kumar, A. Chernatynskiy, M. Hybertsen, R. Hennig, S.R. Phillpot, S.B. Sinnott, "Site-preference of Co and Ti in a quaternary alloy system of Ni_3Al(Co,Ti): Concentration and Temperature effects" (in preparation)
37. S. R. Broderick, A. Kumar, A.A. Oni, J. LeBeau, S.B. Sinnott and K. Rajan, "Assessment of site occupancy of dopants in Ni_3Al: An integrated first principles, statistical learning and atomic imaging study" *Acta Mat* (To be submitted)
38. A. A. Oni, J. H. Dycus, E. Young, K. Rajan and J. M. LeBeau, "Effect of alloy composition on Co site preference in Ni_3Al intermetallic compound" *Intermetallics* (Submitted)
39. S. Broderick, S. Ganguly, K. Rajan, "High throughput computational library of chemistry-modulus relationships in L12 intermetallics via ensemble data mining DOS spectra", *Physica B* (submitted)

Invited Presentations:

Iowa State University:

Krishna Rajan:

1. Informatics : a new paradigm for materials science : World Materials Research Institutes Forum – Lawrence Livermore National Lab. Sept. 15th 2015
2. Materials Cartography- Mapping Chemical Design Pathways: AIChE Annual Meeting , Salt Lake City UT, Nov. 11th 2015
3. Charting the Electronic/Crystal Structure Nexus thru Big Data Analytics: CECAM meeting , Lausanne, Switzerland ; Dec. 2nd 2015\
4. Harnessing Big Data for Computational Design of Ceramics
   Electronic Materials and Applications Conference 2015 - American Ceramic Society
   Orlando FL; January 23rd 2015
5. Materials Informatics and Integrated Computational Materials Engineering
   SAMPE Annual Meeting ,
   Baltimore MD ; May 20th 2015
6. Exploring the Topology of Data in Materials Science
   Workshop on Machine Learning for Many-Particle Systems
   Institute for Pure and Applied Mathematics – UCLA February 25th 2015
7. Informatics for Materials Genomics
   Department of Materials Science
   University of Connecticut, Storrs, CT; September 27, 2013
8. Materials Informatics: a Lecture Series "Cooperation of Computational Materials Science & Mathematics-Towards Smart Materials Design" Symposium Japan Science and Technology Agency; Tokyo, Japan; January 6-10, 2014.
9. Exploring Data Topology for Materials Discovery
   Symposium on Data Analytics for Material Science and Manufacturing
   TMS Annual Meeting, San Diego; February 17-20, 2014
10. NIMS Presidential Lecture – Materials Informatics and the Materials Genome
    National Institute for Materials Science
    Tsukuba, Japan: March 19th 2014
11. Linking Data to Chemistry and Physics of Materials via Informatics
    Workshop on "From Physics and Chemistry to Data Analysis and Back
    St. Petersburg, Russia; June 16th-20th 2014
12. High Dimensional Analysis of Chemically Complex Alloys
    Intl Workshop – Compositionally Complex Alloys 2014
    Munich Germany; July 17th 2014
13. Discovering Materials Science through Data Science
    Department of Materials Science and Engineering
    Carnegie Mellon University
    Pittsburgh PA. September 14th 2012
14. Informatics for Discovering the Materials Genome
    Scientific Discovery Initiative Seminar Series
    Pacific Northwest National Laboratory
    Richland WA. September 19th 2012
15. Expanding the Design Limits in Materials via Data Mining

Symposium on Data Science Approaches for Mechanics of Materials
22nd International Workshop on Computational Mechanics of Materials
Baltimore Sept. 24-26th 2012

16. Informatics for the Inverse Design of Materials
    49th Annual Society of Engineering Science Meeting
    Atlanta GA; October 10-12, 2012
17. "omics" for Materials Science via Informatics
    Symposium on Materials Informatics
    Materials Research Society Fall 2012 meeting, Boston MA; Nov. 26th-30th 2012
18. Materials Co-Design for Translational Breakthroughs in Technology
    Workshop on New and Novel Processes that are on the Verge of Industrial Modernization - Defense Materials Manufacturing and Infrastructure
    National Academy of Sciences, Washington DC ; December 5th 2012
19. Grand Challenges in Computational Materials Design Workshop
    North Carolina State University, Raleigh, NC; Jan. 15-16th 2013
20. Mapping the Materials Genome Landscape
    1st International Conference on Molecular and Materials Informatics
    Melbourne, Australia, February 4-6, 2013
21. Mapping the Electronic Structure Landscape for Materials Discovery
    German Physical Society (DPG) meeting, Regenseberg, Germany, March 15th 2013
22. Enabling ICSME through Informatics and Big Data
    Air Force Research Laboratory- Materials and Manufacturing Directorate
    Wright Patterson Air Force Base, Dayton OH, March 20th 2013
23. Informatics Aided Discovery of Energy Materials
    2013 Kentucky Workshop on Renewable Energy and Energy Efficiency
    Louisville, KY, March 25th 2013
24. Discovering Classfiers in Materials Science through Statistical Learning
    Workshop on Machine Learning and Materials Science
    Santa Fe Institute, Santa Fe, NM, April 3rd 2013
25. Nanoinformatics for Materials Design
    NSF Workshop - Cyberinfrastructure for Environmental Nanoinformatics
    Center for Environmental Implications of Nanotechnology –UCLA
    Los Angeles, CA, May 7th 2013
26. Informatics for Ceramic Crystal Chemistry
    Ceramics by Genome Symposium
    10th Pacific Rim Conference on Ceramic and Glass Technology
    San Diego, CA, June 6th 2013
27. Statistical Learning Guided Design of Materials
    Fritz Haber Institute – Theory Group
    Berlin , Germany, June 17th 2013
28. Developing Property Maps to Guide Materials Design via Statistical Learning
    Summer Research Group Meeting – Materials by Design

Los Alamos National Laboratory, July 17, 2013

29. Big Data for Materials Science
    National Institute for Aerospace Seminar Series: Big Data, Deep Analytics, and Machine Intelligence NASA/ Hampton VA, September 23rd 2013

Florida International University:

1. S.V.Raju and S. K. Saxena,
   Crystal Structure of Ni_3Al with and without RARE-EARTH additions at high temperatures,
   SAMPE Technical Paper at CAMX conference,
   Orlando, Florida, October 13-16, 2014
2. S.V. Raju, M. Page, V. Drozd, V. Rao, S. Saxena,
   Synthesis and phase stability of Ni-Al-Co-Ti super alloys at high pressure using laser heating in DAC", Workshop on high-pressure time-resolved synchrotron techniques,
   September 25-27, 2014Advanced Photon Source, Argonne National Laboratory
3. S.V. Raju, M. Page, V. Drozd, V. Rao, S. Saxena, **"**Strength of Ni-Al alloys under stress**",** poster presented at Advanced Light Source, User meeting Oct 7-9th, (2013) LBNL, Berkeley, USA
4. R. N. Moshaie, V. Drozd, A. Durygin, S. V. Raju, S. K. Saxena, B. Boesl' "Structural Change in Ni-Mn Ga Intermeallic under Stress and Pressure", MRS Spring Meeting & Exhibit. April 21-25, 2014 San Francisco, California.
5. Surendra Saxena, Melting of several elements at high pressures, XV Liquid and Amorphous Metals Conference - Beijing, September 16th, 2013
6. S.V. Raju, B. K. Godwal, J. Yan, S. K .Saxena**, "**Strength of Ni-Al alloys under stress**",** poster presented at Advanced Light Source, User meeting Oct 7-9th, (2013) LBNL, Berkeley, USA
7. R. N. Moshaie, V. Drozd, A. Durygin, S. V. Raju, S. K. Saxena, B. Boesl' "Structural Change in Ni-Mn-Ga Intermeallic under Stress and Pressure", MRS Spring Meeting & Exhibit. April 21-25, 2014 San Francisco, California.

North Carolina State University:

James LeBeau

1. Accurate and precise direct atomic scale crystallography by electron microscopy,
   University of Delaware, (2015).
2. J. M. LeBeau, New frontiers of materials characterization at the atomic scale,
   Yale, (2015).
3. J. M. LeBeau, New frontiers of materials characterization at the atomic scale,
   Eastman Chemical Company, (2015).
4. J. M. LeBeau, Quantifying the whole stem image: where we are and where to go from here,

Joint NSRC Workshop: Big, Deep, And Smart Data Analytics In Materials Imaging, (2015).

5. J. M. LeBeau, J. Houston Dycus, R. M. White, J. M. Pierce, and R. Venkatasubramanian, Resolving ambiguities at interfaces with atomic resolution x-ray spectroscopy, Materials Science & Technology, (2014).
6. New frontiers of materials characterization at the atomic scale, Department of Materials Science & Engineering, Carnegie Mellon University, (2014).
7. New frontiers of atomic scale structural and chemical characterization, Physics Department, University of Texas: Arlington, (2014)
8. From intensity To Distance: Quantifying your STEM Images, Aberration Corrected Microscopy Focused Interest Group, Microscopy & Microanalysis Conference (2014)
9. Structure and chemistry at the atomic scale new paradigm in materials characterization, Department of Materials Science & Engineering, University of Michigan, (2013).

University of Florida

1. Atomic scale investigation of Ni_3AlX alloys using a combined first-principles and statistical learning approach - Aakash Kumar, Scott R. Broderick, Aleksandr Chernatynskiy, Krishna Rajan, Simon R. Phillpot and Susan B. Sinnott (presentation)
   Symposium: Computational Modeling and Stochastic Methods for Materials Discovery and Properties, TMS annual meeting, Orlando, FL, Mar 2015
2. Atomic scale investigation of Ni_3AlX alloys using a combined first-principles and statistical learning approach - Aakash Kumar, Scott S. Broderick, Aleksandr Chernatynskiy, Adedapo Oni, James M. LeBeau, Krishna Rajan, Simon R. Phillpot and Susan B. Sinnott (presentation)
   Symposium: Informatics and Genomics for Materials Development, MRS fall meeting, Boston, MA, Dec 2014
3. Rare-earth element alternatives in alloy design: Contributions from first-principles calculations- Susan B. Sinnott, Aakash Kumar, Srikant Srinivasan, Scott R. Broderick and Krishna Rajan (Invited talk) Symposium: Computational Discovery of Materials, TMS annual meeting, San Diego, CA Feb 2014
4. Atomic scale investigation of Ni_3AlX alloys using a combined first-principles and statistical learning approach – Aakash Kumar, Scott R. Broderick, Minki Hong, Krishna Rajan, Simon R. Phillpot and Susan B. Sinnott (poster) Conference: Information Science for Materials Discovery and Design, Centre for Nonlinear studies, Los Alamos National Laboratory, Santa Fe, NM, Feb 2014
5. Applications of Computational Methods to Materials Design and Discovery, Susan Sinnott, AVS 60, Long Beach, October 31, 2013
6. Rare-earth Element Alternatives in Alloy Design: Contributions from First-principles Calculations Susan Sinnott, Symposium on Computational Discovery of Novel Materials TMS Annual Meeting, San Diego; February 17-20, 2014
7. Expanding the Toolbox: Design and Discovery using Material Modeling Methods
   Susan Sinnott, Distinguished Lecture in Nanotechnologies through Materials Innovation
   Northeastern University in Boston, Massachusetts, April 3, 2014

8. **(Keynote)** Expanding the Toolbox: Design and Discovery using Material Modeling Methods
   Susan Sinnott, Florida American Vacuum Society Chapter Meeting
   Orlando, Florida, March 3, 2014
9. Advanced Approaches for Material Design and Discovery
   Susan Sinnott, Defense Materials Manufacturing and Infrastructure (DMMI) Workshop on Materials State Awareness, Washington, DC, August 6-7, 2014

Changes in research objectives : None

Change in AFOSR Program Manager : None

Extensions granted or milestones slipped : None

AFOSR Deliverables Submission Survey

Response ID:5823 Data

1.

1. Report Type

Final Report

Primary Contact E-mail
Contact email if there is a problem with the report.

krajan3@buffalo.edu

Primary Contact Phone Number
Contact phone number if there is a problem with the report

716-645-1380

Organization / Institution name

Iowa State University

Grant/Contract Title
The full title of the funded effort.

SUSTAINABLE ALLOY DESIGN: SEARCHING FOR RARE EARTH ELEMENT ALTERNATIVES THROUGH CRYSTAL ENGINEERING

Grant/Contract Number
AFOSR assigned control number. It must begin with "FA9550" or "F49620" or "FA2386".

FA9550-12-1-0456

Principal Investigator Name
The full name of the principal investigator on the grant or contract.

Krishna Rajan

Program Manager
The AFOSR Program Manager currently assigned to the award

Ali Sayir

Reporting Period Start Date

11/15/2012

Reporting Period End Date

11/14/2015

Abstract

The objective of this project was to identify new chemical substitutions for rare earth elements in high temperature alloys via an informatics based alloy design strategy that captures the "rational materials design" strategy by integrating atomistic and multi-scale modeling with unique synthesis and characterization experiments under extreme pressure / temperature conditions. We have successfully achieved the primary goal of this project by identifying 29 new rare earth free Co-based and Ni-based superalloys. This provides for the first time a pathway for searching and identifying elemental substitutions in alloy design that now offers a means for significantly enhancing the acceleration of new critical element substitutions. This BRI sponsored project has also established a new data driven methodology tracking the collective influence of the multiple attributes of alloying elements on both thermodynamic and mechanical properties of metal alloys. The search for elemental

substitutions and/or additions needed to refine metal alloy compositions and enhance their properties is a classical problem in metallurgical alloy design. Finding appropriate alloy chemistries based on a systematic exploration using either computational and/or experimental approaches is often guided by prior heuristic knowledge that harnesses expected trends captured in the periodic table that can influence phase stability and properties. A major transformative result from this project is that we have for the first time established a unified mathematical formalism for identifying the pathways of chemical design of alloys that can simultaneously capture the complexity of interactions of metrics associated with thermodynamics, crystal structure and microstructure. The implication of our work goes beyond the immediate goals of this project by providing a computational framework that is generic enough to integrate data from many different length scales and as such can accommodate the addition of data associated with microstructure, processing and environmental response of alloys. This approach can be applied to many material systems and design objectives important to the Air Force. This is project has also demonstrated how informatics methods can help integrate data from computational materials science modeling, imaging and materials characterization techniques This project has also made significant contributions in advancing methodology and technique based research including: high throughput first principles calculations, ultra-high resolution quantitative correlative microscopy (integrating STEM and APT) and in –situ property characterization (high pressure/ high temperature X-ray studies).

Distribution Statement
This is block 12 on the SF298 form.

Distribution A - Approved for Public Release

Explanation for Distribution Statement
If this is not approved for public release, please provide a short explanation. E.g., contains proprietary information.

SF298 Form
Please attach your SF298 form. A blank SF298 can be found here. Please do not password protect or secure the PDF The maximum file size for an SF298 is 50MB.

SF-298.pdf

Upload the Report Document. File must be a PDF. Please do not password protect or secure the PDF . The maximum file size for the Report Document is 50MB.

AFOSR-BRI_ final-report.pdf

Upload a Report Document, if any. The maximum file size for the Report Document is 50MB.

Archival Publications (published) during reporting period:

1. Information-driven Approaches to Materials Discovery and Design Eds. T. Lookman, F. Alexander and K.Rajan: Springer Series in Materials Science (2016)
2. S.R. Broderick and K. Rajan "Discovering Electronic Signatures for Phase Stability of Intermetallics via Machine Learning" in Information-driven Approaches to Materials Discovery and Design Eds. T. Lookman, F. Alexander and K.Rajan: Springer Series in Materials Science, Ch. 12 (2016)
3. F Vurpillot, W.Lefebvre, J.M. Cairney, C. Oberdorfer, B.P. Geiser and K. Rajan. "Advanced volume reconstruction and data mining methods in atom probe tomography" MRS Bulletin 41, 46-52 (2016)
4. A. J. Zaddach, C. Niu, A. A. Oni, M. Fan, J. M. LeBeau, D. L. Irving, C. C Koch. "Structure and magnetic properties of a multi-principal element Ni-Fe-Cr-Co-Zn-Mn alloy" Intermetallics 68, 107-112 (2016)
5. O.Wodo , S. Broderick and K. Rajan, " Microstructural Informatics to Driven Rational Materials Design", MRS Bulletin (August 2016- in press)
6. S. Broderick and K. Rajan , ""Harnessing the BigData Paradigm for ICME: transforming from materials selection to materials enabled design" JOM- TMS Journal of Metals, Minerals and Materials Society (August 2016 – in press)
7. S. Srinivasan, S.R. Broderick, R. Zhang, A. Mishra, S.B. Sinnott, S.K. Saxena, J.M. LeBeau, K. Rajan. "Mapping Chemical Selection Pathways for Designing Multicomponent Alloys: An Informatics Framework for Materials Design." Nature Scientific Reports, 5, 17960 (2015)
8. S. Srinivasan, K. Kaluskar, S. Broderick, K. Rajan. "Extracting Features Buried within High Density Atom Probe Point Cloud Data through Simplicial Homology." Ultramicroscopy 159, 374-380 (2015)

9. S. Srinivasan, K. Kaluskar, R. Dumpala, S. Broderick, K. Rajan. "Automated Voxelation of 3D Atom Probe Data through Kernel Density Estimation." Ultramicroscopy 159, 381-386 (2015)
10. C.S. Kong, S.R. Broderick, T.E. Jones, C. Loyola, M.E. Eberhart, K. Rajan. "Mining for Elastic Constants of Intermetallics from the Charge Density Landscape." Physica B. 458, 1-7 (2015)
11. C. Niu, A. J. Zaddach, A. A. Oni, X. Sang, J. W. Hurt III, J. M. LeBeau, C. C. Koch, D. L. Irving, "Spin-driven Ordering of Cr in the Equiatomic High Entropy Alloy NiFeCr", Applied Physics Letters, 106, (161905) 2015
12. A. A. Oni, X. Sang, S. V. Raju, S. Dumpala, S. Broderick, A. Kumar, S. B. Sinnott, S. K. Saxena, K. Rajan, J. M. LeBeau, "Large Area Strain Analysis Using Scanning Transmission Electron Microscopy Across Multiple Images" Applied Physics Letters, 106, (011601) 2015.
13. C.S. Kong, S.R. Broderick, T.E. Jones, C. Loyola, M.E. Eberhart, K. Rajan. "Mining for Elastic Constants of Intermetallics from the Charge Density Landscape." Physica B. 458, 1-7 (2015)
14. S.V. Raju, A. A. Oni¬¬,¬ B. K. Godwal, J. Yan, V. Drozd, S.Srinivasan, J. M. LeBeau, K.Rajan, S. K .Saxena,"Effect of B and Cr on elastic strength and crystal structure of Ni3Al alloys under high pressure", J. of Alloys and Compounds 619 (2015) 616-620 .
15. S.V. Raju, B.K. Godwal, J. Yan, R. jeanloz, S.K. Saxena, "Yield strength of Ni-Al-Cr superalloy under presuure.", J. Alloys and Compounds 657 (2015) 889-892.
16. A. Kumar at al., "Charge optimized many-body (COMB) potential for dynamical simulation of Ni–Al phases", J. Phys. Cond. Matt. 27, 336302 (2015)
17. A. Kumar, A. Chernatysnkiy, M. Hong, S.R. Phillpot and S.B. Sinnott, "An ab initio investigation of the effect of alloying elements on the elastic properties and magnetic behavior of Ni3Al", Comput. Mater. Sci., 101, 39-46 (2015)
18. S.V. Raju, Z. Geballe, B.K. Godwal, B. Kalkan, Q. Williams, R. Jeanloz,, "High Pressure and Temperature structure of Liquid and Solid Cd: Implications for the melting curve of Cd" Materials Research Express (2014) 046502
19. S.Broderick, U. Ray, S. Srinivasan, K. Rajan, G. Balasubramanian, "An Informatics Based Analysis of the Impact of Isotope Substitution on Phonon Modes in Graphene", Applied Physics Letters 104, 243110 (2014)
20. S. Dumpala, S.R. Broderick, P.A.J. Bagot, K. Rajan, "An Integrated High Temperature Environmental Cell for Atom Probe Tomography Studies of Gas-Surface Reactions: Instrumentation and Results", Ultramicroscopy 141, 16-21 (2014)
21. R. F. Zhang and K.Rajan, "Statistically Based Assessment of Formation Enthalpy for Intermetallic Compounds"; Chem.Phys. Lett. 612, 177-181 (2014)
22. Informatics for Materials Science and Engineering: editor Krishna Rajan ; Elsevier ISBN: 9780123943996 (2013)
23. S. Kalavathi, S.V. Raju, Q. Williams, P Ch Sahu, V S Sastry and H K Sahu, "Pressure-induced frustration in charge ordered spinel AlV2O4", J. Phys.: Condens. Matter 25 292201 (2013).
24. Z.M. Geballe, S.V. Raju, B.K. Godwal and R. Jeanloz, "Clapeyron slope reversal in the melting curve of AuGa2 at 5.5 GPa", J. Phys.: Condens. Matter 25 415401 (2013).
25. S.B. Sinnott, "Material Design and Discovery with Computational Materials Science", J. Vac. Sci. Technol. A 31, 050812 (2013)
26. S.R. Broderick, A. Bryden, S.K. Suram, "Data Mining for Isotope Discrimination in Atom Probe Tomography." Ultramicroscopy, 132, 121-128 (2013)
27. J. Peralta, S.R. Broderick, K. Rajan. "Mapping Energetics of Atom Probe Evaporation Events through First Principles Calculations." Ultramicroscopy, 132, 143-151 (2013)
28. A. Bryden, S. Broderick, S.K. Suram, K. Kaluskar, R. LeSar, K. Rajan. "Interactive Visualization of APT Data at Full Fidelity." Ultramicroscopy, 132, 129-135 (2013)
29. S.K. Suram, K. Rajan. "Calibration of Reconstruction Parameters in Atom Probe Tomography Using a Single Crystallographic Orientation." Ultramicroscopy, 132, 136-142 (2013)
30. S.Broderick, S.Srinivasan, R. Zhang and K.Rajan: "Identification of Critical Element Substitutes for Ni Based Superalloy Design via Manifold Learning" Proc. National Academy of Sciences (submitted)
31. S.K. Saxena, S.V. Raju, K. Rajan, S. Broderick. "Searching L12 phase in ternary and quaternary super alloy compositions (Ni-Al-Co-Ti)" Calphad (submitted)
32. S.V. Raju, B. K. Godwal, S. Srikant, J. Yan, K. Rajan and S. K .Saxena, "Strain variation across lattice planes of Ni3Al:B(500ppm) as a function of applied load". (In preparation).
33. S.V.Raju, R. Hrubiak, V.Drozd, S. K .Saxena, "Phase stability of Ni-Co-Ti-Al based L12 superalloys with varying composition of Co", Appl. Phys. Lett.(To Submit).
34. S.V. Raju, B. K. Godwal, J. Yan, S. K .Saxena, "Yield strength of Cr doped Ni3Al from hydrostatic and non-hydrostatic compression", J. Alloys and Compounds (Under Review).

35. A. Kumar, T. Liang, A. Chernatynskiy, S.R. Phillpot and S.B. Sinnott, "Effect of defects on the strength on Ni3Al-Al2O3 interfaces using Molecular Dynamics studies" (in preparation)
36. A. Kumar, A. Chernatynskiy, M. Hybertsen, R. Hennig, S.R. Phillpot, S.B. Sinnott, "Site-preference of Co and Ti in a quaternary alloy system of Ni3Al(Co,Ti): Concentration and Temperature effects" (in preparation)
37. S. R. Broderick, A. Kumar, A.A. Oni, J. LeBeau, S.B. Sinnott and K. Rajan, "Assessment of site occupancy of dopants in Ni3Al: An integrated first principles, statistical learning and atomic imaging study" Acta Mat (To be submitted)
38. A. A. Oni, J. H. Dycus, E. Young, K. Rajan and J. M. LeBeau, "Effect of alloy composition on Co site preference in Ni3Al intermetallic compound" Intermetallics (Submitted)
39. S. Broderick, S. Ganguly, K. Rajan, "High throughput computational library of chemistry-modulus relationships in L12 intermetallics via ensemble data mining DOS spectra", Physica B (submitted)

Changes in research objectives (if any):

None

Change in AFOSR Program Manager, if any:

None

Extensions granted or milestones slipped, if any:

None

AFOSR LRIR Number

LRIR Title

Reporting Period

Laboratory Task Manager

Program Officer

Research Objectives

Technical Summary

Funding Summary by Cost Category (by FY, $K)

	Starting FY	FY+1	FY+2
Salary			
Equipment/Facilities			
Supplies			
Total			

Report Document

Report Document - Text Analysis

Report Document - Text Analysis

Appendix Documents

2. Thank You

E-mail user

Feb 13, 2016 20:22:09 Success: Email Sent to: krajan3@buffalo.edu

Response ID: 5823

Survey Submitted:	Feb 13, 2016 8:22 PM
IP Address:	74.77.229.77
Language:	English (en-US,en;q=0.5)
User Agent:	Mozilla/5.0 (Windows NT 6.1; rv:43.0) Gecko/20100101 Firefox/43.0
Http Referrer:	http://afosr.reports.sgizmo.com/s3/
Page Path:	1 : (SKU: 1) 2 : Thank You (SKU: 2)
SessionID:	1455411180_56bfcfec121040.78762797

Response Location

Country:	United States
Region:	NY
City:	Lancaster
Postal Code:	14086
Long & Lat:	Lat: 42.905700683594, Long:-78.626403808594